

**UCSF**

**UC San Francisco Electronic Theses and Dissertations**

**Title**

Endocrine Control of Heart Regeneration in Evolution and Development

**Permalink**

<https://escholarship.org/uc/item/5xd6h28v>

**Author**

Cutie, Stephen

**Publication Date**

2021

Peer reviewed|Thesis/dissertation

Endocrine Control of Heart Regeneration in Evolution and Development

by  
Stephen Cutie

DISSERTATION  
Submitted in partial satisfaction of the requirements for degree of  
DOCTOR OF PHILOSOPHY

in  
Bioengineering

in the  
GRADUATE DIVISION

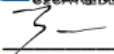
of the  
UNIVERSITY OF CALIFORNIA, SAN FRANCISCO  
AND  
UNIVERSITY OF CALIFORNIA, BERKELEY

Approved:

DocuSigned by:  
  
9B89D521CB8C475... Guo Huang  
Chair

DocuSigned by:  
  
DocuSigned by: 43C... Irina Conboy

  
DocuSigned by: 4DD... Hao Li

  
DocuSigned by: 4DD... Zev Gartner  
5C989DB09166439...

Committee Members



## ACKNOWLEDGEMENTS

This thesis work would not have been possible without the invaluable insight and training of my PI, thesis advisor, and graduate mentor: Guo Huang. I am beyond grateful for the relentless optimism, the troubleshooting expertise, and above all the dynamic and dedicated support that have defined his mentorship these last four years.

I also thank former post-docs Alex Payumo and Kentaro Hirose for their guidance and assistance with many of the techniques required to bring this thesis to fruition; former undergraduate researcher Alexander Amram for substantial contributions to proliferation analysis of CMs both *in vitro* and *in vivo*; as well as current and former lab members Rachel Bigley, Alison Hoang, Xi Chen, Xiaoxin Chen, Nevan Powers, Shea Khyeam, David Xia-Zhu, and Dominic Lunn for their technical assistance throughout my time in the Huang Lab.

Lastly, I thank A. Arnold for sharing PS121912 with our lab, Gabriela Greenland for her consistent guidance and support as a peer, and each member of my thesis committee beyond my advisor – Irina Conboy, Hao Li, and Zev Gartner – for their expertise and service. I will also be eternally grateful to the family members without whom I would not have come within miles of graduate school: my parents, my siblings, and my tia.

Funding: This work has been supported by a NIGMS IMSD fellowship, Hillblom fellowship, and NIH F31 predoctoral fellowship (to S.C.), a UCSF-IRACDA postdoctoral fellowship (to A.P.), NIH (R01HL13845) Pathway to Independence Award (R00HL114738), Edward Mallinckrodt Jr. Foundation, March of Dimes Basil O'Conner Scholar Award, American Heart Association Beginning Grant-in-Aid, American Federation for Aging Research, Life Sciences Research Foundation, Program for Breakthrough Biomedical Research, UCSF Eli and Edythe Broad Center of Regeneration Medicine and Stem Cell Research Seed Grant, UCSF Academic Senate Committee on Research, REAC Award (Harris Fund), Department of Defense, and Cardiovascular Research Institute (to G.N.H.).

# Endocrine Control of Heart Regeneration in Evolution and Development

Stephen Cutie

## Abstract

Cardiac regenerative potential varies considerably across and within vertebrate species. Heart regeneration is an ancestral trait that is lost both as more recent vertebrate lineages evolved to adapt to new environments and selective pressures, and as members of certain species developmentally progress towards their adult forms. While lower vertebrates and neonatal mammals retain robust capacities for cardiomyocyte (CM) proliferation and cardiac regeneration, adult mammalian CMs lose proliferative potential due to cell-cycle withdrawal and polyploidization, failing to mount a proliferative response to regenerate lost myocardium after cardiac injury. The decline of murine CM proliferative potential occurs in the neonatal period when the endocrine system undergoes drastic changes for adaptation to extrauterine life. Here, we demonstrate that thyroid hormone (TH) signaling functions as a primary factor driving CM proliferative potential loss in vertebrates, able to shut down regeneration when present and enhance regeneration when absent. Furthermore, we implicate thyroid hormone as a critical driver of endothermy acquisition as well as CM cell cycle exit. We also show that agonists of glucocorticoid receptor (GR) and vitamin D receptor (VDR) suppressed neonatal CM proliferation *in vitro*. We examined CM nucleation and proliferation in neonatal mutant mice lacking GR or VDR specifically in CMs, but we observed no difference between mutant and control littermates. Additionally, we generated compound mutant mice that lack GR or VDR and express dominant-negative TH receptor alpha in their CMs, and similarly observed no increase in neonatal CM proliferative potential compared to dominant-negative TH receptor alpha mice alone. Thus, although GR and VDR activation in cultured neonatal CMs is sufficient to inhibit CM proliferation, they seem to be dispensable for neonatal CM cell-cycle exit and binucleation *in vivo*. Our results suggest distinct roles for several endocrine players in governing cardiac regenerative potential in vertebrates.

## Table of Contents

<b>Introduction: Cardiac regeneration in vertebrates .....</b>	<b>1</b>
Lower vertebrates can regenerate myocardium as adults.....	1
Mammals can transiently regenerate myocardium as neonates, but cannot as adults .....	2
CM polyploidization shuts down vertebrate cardiac regenerative potential .....	4
<b>Chapter I – Elucidating the evolutionary and developmental role of</b>	
<b>Thyroid Hormone in cardiac regeneration .....</b>	<b>6</b>
Exogenous thyroid hormone suppresses cardiac regenerative potential in zebrafish.....	6
Loss of thyroid hormone signaling enhances heart regenerative potential in mice .....	7
<b>Chapter II – Studying the Roles of Glucocorticoid and Vitamin D Signaling</b>	
<b>on Cardiomyocyte Proliferative Potential .....</b>	<b>8</b>
Glucocorticoid and vitamin D receptor activation inhibit	
neonatal mouse cardiomyocyte proliferation in vitro. ....	9
Glucocorticoid and vitamin D receptors in cardiomyocytes are dispensable for the	
regulation of neonatal mouse cardiomyocyte proliferation and binucleation in vivo.....	10
Loss of glucocorticoid or vitamin D receptor does not enhance cardiomyocyte	
proliferation potential in mice with deficiency in thyroid hormone signaling in vivo. ....	11
<b>Chapter III – Further Exploration of Thyroid Hormone Physiology .....</b>	<b>13</b>
Thyroid hormone signaling and endothermy acquisition .....	14
LRRC15: a target of thyroid hormone signaling? .....	16
CM polyploidization shuts down vertebrate cardiac regenerative potential .....	16
<b>Conclusion, Discussion, and Perspectives.....</b>	<b>17</b>
<b>Figures.....</b>	<b>21</b>

<b>Methods</b> .....	<b>37</b>
<b>References</b> .....	<b>43</b>

**List of Figures**

Figure 1.1 .....21

Figure 1.2 .....22

Figure 1.3 .....23

Figure 2.1 .....24

Figure 2.2 .....25

Figure 2.3 .....26

Figure 2.4 .....27

Figure 2.5 .....28

Figure 2.6 .....29

Figure 2.7 .....30

Figure 2.8 .....31

Figure 2.9 .....32

Figure 2.10 .....33

Figure 2.11 .....34

Figure 3.1 .....35

Figure 3.2 .....36



## **Introduction: Cardiac regeneration in vertebrates**

Cardiovascular disease is the leading killer in the United States, mostly due to heart failure after myocardial infarction (MI)<sup>1,2</sup>. After ischemic injury like MI induces CM death in the hearts of adult mammals, lost CMs are not replenished and fibrotic tissue permanently replaces previously functional cardiac muscle. However, lower vertebrates like zebrafish (*Danio rerio*), newts (*Notophthalmus viridescens*), axolotls (*Ambystoma mexicanum*), and some frogs (*Xenopus tropicalis*) display robust CM proliferation and myocardial regeneration after cardiac injury<sup>2-5</sup>.

### ***i. Lower vertebrates can regenerate myocardium as adults***

Adult zebrafish can fully regenerate the myocardium. Resection of up to 20% of the *D. rerio* ventricle induces a robust proliferative response in the myocardium by 14 days post-injury and temporary fibrosis that resolves with complete regeneration and no scar by 60 days post-injury<sup>6</sup>. Lineage-tracing confirmed that zebrafish cardiac regeneration occurs via dedifferentiation and proliferation of pre-existing cardiomyocytes (CMs) after injury<sup>7,8</sup>. Intriguingly, this complete cardiac regenerative potential in the zebrafish can be blunted by physiological stress<sup>9</sup>, inhibition of vitamin D signaling<sup>10</sup>, and artificial polyploidization of the myocardium<sup>11</sup>. Additionally, like their zebrafish relatives, the adult giant danio *Danio aequipinnatus* can fully regenerate myocardium after cautery injury, clearing all local necrosis and fibrosis by 60 days post-injury<sup>12</sup>.

Similarly, newt cardiac regenerative potential rivals that of zebrafish. Resection of up to 10% of the *Notophthalmus viridescens* ventricle induces myocardial cell proliferation and resolves as complete ventricular regeneration by 70 days post-injury<sup>3</sup>. CM proliferation of the predominantly mononuclear diploid variety is observed during newt cardiac regeneration<sup>13,14</sup>. Newt CM plasticity even allows CMs transplanted into regenerating limb buds to transdifferentiate and express skeletal muscle and chondrocyte markers<sup>15</sup>. The gene expression profile of the regenerating newt heart differs from regenerative expression profiles in other

organs<sup>16</sup>.

Alongside newts and zebrafish, in the adult *Ambystoma mexicanum*, both ventricular resection<sup>17</sup> and cryoinjury<sup>18</sup> of the myocardium induce CM proliferation and complete cardiac regeneration and restoration of heart function within 90 days post-injury, without permanent fibrosis. Notably, successful heart regeneration in the axolotl depends not only on the induction of CM proliferation after injury, but also on macrophage activity. Upon macrophage depletion, myofibroblasts induce excessive collagen deposition that results in permanent fibrosis<sup>18</sup>.

Evidence also exists of at least partial myocardial regeneration in adult frogs. Early work in *Rana temporaria* observed a partial regenerative response after crush injury of the ventricle, with a post-injury induction of CM proliferation<sup>19</sup> and subsequent sinus rhythm restoration to nearly 80% of animals within 200 days post-injury<sup>20</sup>. Furthermore, adult 1-year-old *Xenopus tropicalis* hearts mount a robust CM proliferative response to 10% apical resection that fully regenerates the lost myocardium nearly scar-free by 30 days after injury<sup>5</sup>. However, adult cardiac regenerative potential seems to vary among different frog species: research in *X. laevis* indicates that while tadpoles induce CM proliferation after oxidative damage<sup>21</sup> and also mount a complete regenerative response after resection, post-metamorphosis 6-month old juveniles and 5-year-old adults can only mount a partial regenerative response to comparable apical resection<sup>22,23</sup>. While this discrepancy between *X. tropicalis* and *X. laevis* may be explained by the different ages of the resected adults, it may also be explained by ploidy differences between the two species: *X. tropicalis* has a diploid genome with mostly mononuclear CMs, but *X. laevis* has a pseudotetraploid genome with mostly tetraploid CMs<sup>24</sup>. Further work may shed more light about this differential regenerative potential. It is not unprecedented for related species to have radically different cardiac regenerative capacities, as with zebrafish and medaka<sup>25</sup>.

**ii. Mammals can transiently regenerate myocardium as neonates, but cannot as adults**

Intriguingly, while cardiac regeneration has not been observed in adult mammals,

neonatal mammals transiently possess considerable CM proliferative and regenerative potential. However, this transient CM proliferative potential is lost as neonatal CMs binucleate and permanently exit the cell cycle<sup>26,27</sup>. This transience is evident in mice. While adult *Mus musculus* are incapable of myocardial regeneration after cardiac injury, complete cardiac regeneration without permanent fibrosis is possible during embryonic and neonatal stages<sup>28,29</sup>. Resection of ~15% of the ventricular apex in P0 mice induces cardiomyocyte (CM) proliferation that regenerates the lost myocardium without evidence of permanent fibrosis or compromised cardiac function by 21 days post-resection<sup>28</sup>. Similarly, ischemic cardiac damage caused by permanent ligation of the left anterior descending coronary artery (LAD) in P1 mice resolves as fully-regenerated cardiac muscle without evidence of fibrosis by 21 days post-ligation<sup>29</sup>. In both cases, CMs in the regenerated myocardium came from pre-existing CMs that were induced to dedifferentiate and proliferate after injury, and the neonatal regenerative response was lost by P7<sup>28,29</sup>. This closure of the murine neonatal regenerative window between birth and P7 coincides with the developmental polyploidization of the neonatal myocardium during the first week of life, during which >90% of CMs binucleate and permanently exit the cell cycle<sup>26,27</sup>.

As with mice, a transient neonatal cardiac regenerative response has been observed in *Rattus norvegicus*. In P1 rats, 18% apical resection induced myocardial regeneration including robust, uniform troponin I deposition and Connexin 43 expression, as well as restoration of baseline cardiac function and perfusion by 60 days post-injury<sup>30</sup>. However, this robust regenerative response was lost by P7, in which permanent apical scar tissue formed and cardiac function did not fully recover<sup>30</sup>. Neonatal rats have also been observed to mount a regenerative response to burn lesions made in the myocardium<sup>31</sup>.

Myocardial infarction also induces a robust but transient regenerative response in *Sus domesticus*. Cardiac injury in P2 pigs induces CM proliferation that regenerates the lost myocardium and restores cardiac function without permanent fibrosis by 12 weeks post-injury<sup>32</sup>. P1 pigs fully regenerate from myocardial infarction even more rapidly, within 30 days<sup>33</sup>.

However, this porcine regenerative response is progressively lost by P14<sup>32,33</sup>. P3 pigs maintain substantial fibrosis at 30 days post-injury<sup>33</sup> and fibrosis is still observed at 12 weeks post-injury<sup>32</sup>, suggesting that the porcine neonatal regenerative window closes very soon after P2.

Intriguingly, cardiac regeneration has even been anecdotally inferred in neonatal humans. There are documented cases of infants suffering massive myocardial infarctions shortly after birth and yet surviving without apparent long-term deficits in cardiac function<sup>34–37</sup>. One newborn that suffered a severe infarction at birth due to coronary artery occlusion showed normal cardiac function and morphology at one year old<sup>38</sup>. However, post-infarct CM proliferation induction in adult humans is limited<sup>39</sup>. It remains to be established when cardiac regenerative potential is lost in humans.

### ***iii. CM polyploidization shuts down vertebrate cardiac regenerative potential***

While mononuclear diploid CMs and binuclear polyploid CMs proliferate at similar rates *in vitro* when co-cultured with embryonic mouse CMs<sup>40</sup>; *in vivo*, the proliferative potential of the former exceeds that of the latter in the vertebrate myocardium. Because the regeneration-competent hearts of lower vertebrates and neonatal mammals consist predominantly of mononuclear diploid CMs while the non-regenerative hearts of adult mammals consist primarily of polyploid CMs – while cardiac regeneration observed across multiple vertebrate species is consistently mediated by CM proliferation – this developmental and evolutionary CM polyploidization is implicated as a critical inhibitor of CM proliferative potential<sup>4,38,41,42</sup> (**FIG 1A**). This is supported by observations that mouse strains with higher percentages of mononuclear diploid CMs induce more CM proliferation after cardiac injury and are left with smaller fibrotic scars<sup>43</sup>. However, the underlying molecular processes that drive mammalian CM polyploidization and cell cycle withdrawal are not fully understood. Still, because CM ploidy inversely correlates with cardiac regenerative potential, we treated CM ploidy as a proxy for cardiac regenerative potential and screened 41 vertebrate species for the percentage of diploid CMs in their myocardium so we could correlate other physiological attributes against known

cardiac regenerative potential (**FIG 1B**). Of several physiological attributes that we compared against diploid CM percentage, we identified that both vertebrate standard metabolic rate and mammalian body temperature correlate linearly with CM ploidy and used this as the basis for further investigation (**FIG 1C**).

## **Chapter I – Elucidating the evolutionary and developmental role of Thyroid Hormone in cardiac regeneration**

Recent evidence indicates that thyroid hormones (THs) play a crucial role in driving developmental CM polyploidization and suppressing CM proliferative potential in vertebrates across evolution<sup>44</sup>. TH signaling is a critical regulator of metabolism and thermogenesis conserved across vertebrates and is particularly active in endotherms, suspected as a critical driver of the evolutionary ectotherm-to-endotherm transition<sup>45–47</sup>. THs enhance CM contractility *in vivo* and rise soon after birth in neonatal mice, coinciding with the closure of the CM proliferative window<sup>48,49</sup>. Serum TH levels are also substantially lower in newts and zebrafish than in non-regenerative mammals<sup>50,51</sup>. Furthermore, reduced ventricular thyroid hormone signaling, low ventricular triiodothyronine (T3), and increased ventricular thyroxine (T4) due to reduced D2 deiodinase have been documented in both ischemic and dilated cardiomyopathy.<sup>52–</sup>

54

### ***i. Exogenous thyroid hormone suppresses cardiac regenerative potential in zebrafish***

In light of this recent evidence in vertebrates implicating thyroid hormones (THs) in promoting CM polyploidization and cell-cycle exit, we sought to directly interrogate the relationship between TH signaling and CM proliferative potential<sup>44</sup>. We began by assessing whether increasing TH signaling in a vertebrate capable of adult cardiac regeneration could blunt the regenerative response. As previously mentioned, zebrafish can fully regenerate from 20% apical resection at 30 days post-injury, and their regenerative response is driven by a CM proliferative burst that peaks 2 weeks after injury<sup>6</sup>. We performed apical resections on adult zebrafish and allowed them to recover either in standard water or water dosed with thyroid hormone (**FIG 2A**). At 14 days post-injury, those zebrafish dosed with thyroid hormone exhibited a 45% reduction in CM proliferation compared to controls, suggesting a blunted regenerative response (**FIG 2B**). Ultimately, when we examined their hearts at 30 days post-injury – when

scarless regeneration should have been completed – we observed over 5-fold greater retention of fibrotic area and a pronounced failure to fully regenerate the myocardium in the thyroid hormone-treated fish (**FIG 2C**). As such, we concluded that increasing thyroid hormone signaling in a regeneration-competent vertebrate adult was sufficient to suppress CM proliferative potential and inhibit cardiac regeneration<sup>44</sup>.

*ii. Loss of thyroid hormone signaling enhances heart regenerative potential in mice*

Having demonstrated this, we next sought to further explore the converse contribution of thyroid hormone to vertebrate cardiac regeneration: could blunting thyroid hormone signaling in a regeneration-incompetent higher vertebrate affect its cardiac regenerative potential? When we dosed neonatal mice with propylthiouracil (PTU) – a potent inhibitor of TH synthesis – through postnatal day 14 (P14), their myocardia showed significantly increased mononuclear CM percentage and CM proliferation<sup>44</sup> (**FIG 3A**). These mononuclear CMs and CM proliferation phenotypes are also observed in mutant mice in which TH signaling is specifically inactivated in CMs<sup>44</sup> (**FIG 3B**). Both chemical and genetic inhibition of CM thyroid hormone signaling from birth through P14 consistently resulted in approximately 30% retention of mononuclear diploid CMs in the myocardium, as well as over 3-fold increase in proliferating (Ki67+) CMs<sup>44</sup>. These mutant mouse hearts also display enhanced recovery after MI as indicated by cardiac contractile functions and fibrosis one month post-surgery (**FIG 3C**). Taken together with our zebrafish data, these data strongly suggest an inhibitory role played by TH in the developmental control of CM proliferative potential during the neonatal window.

## Chapter II – Studying the Roles of Glucocorticoid and Vitamin D Signaling on Cardiomyocyte Proliferative Potential

In addition to TH, other hormones such as glucocorticoids and vitamin D have been shown to suppress CM proliferation in culture. Glucocorticoids are stress-associated steroid hormones produced by the adrenal glands that act on nearly all organs in the body via binding to the glucocorticoid receptor (GR)<sup>55-57</sup>. Specifically, glucocorticoids like dexamethasone are established cell cycle regulators known to repress the cell cycle primarily through the GR, which acts as a transcription factor after glucocorticoid binding<sup>58,59</sup>. It has been reported that GR activation inhibits neonatal rat CM proliferation, promotes neonatal rat CM hypertrophy, and increases CM binucleation through epigenetic repression of Cyclin D2 gene<sup>60-62</sup>. Furthermore, adult zebrafish heart regeneration is impaired by either GR agonist exposure<sup>63</sup> or crowding-induced stress through GR activation<sup>9</sup>.

Vitamin D is a steroid hormone precursor that is hydroxylated sequentially in the liver and kidneys into ercalcitriol (D2) or calcitriol (D3). These active hormones can bind to vitamin D receptors (VDRs) and regulate downstream gene expression in target cells<sup>64</sup>. Alfacalcidol (Alfa) is a vitamin D analog that forms calcitriol directly after hydroxylation in the liver<sup>65</sup>. Anti-proliferative effects of vitamin D analogs have been reported in mammalian cells generally<sup>66</sup> as well as mammalian CMs and CM-derived cell lines specifically<sup>67,68</sup>. VDR activation reduces expression of both PCNA protein levels and *c-myc* and inhibits proliferation in neonatal rat CM culture<sup>69</sup>. Vitamin D analogs have been reported to inhibit proliferation in mammalian primary CMs and similar cell lines<sup>67,68,70</sup>, but these effects may not be conserved across all vertebrates. Notably, VDR signaling may have distinct regulatory roles across vertebrates. Unlike in mammals, vitamin D analogs alfacalcidol and calcipotriene significantly increase CM proliferation in embryonic zebrafish, whereas VDR-inhibitor PS121912 significantly decreases CM proliferation<sup>10</sup>. Alfacalcidol also stimulates CM proliferation in adult zebrafish during heart regeneration, while VDR suppression decreases CM proliferation during regeneration<sup>10</sup>.



Intriguingly, CM-specific deletion of either GR or VDR promotes cardiac hypertrophy<sup>71-73</sup>. This cardiac enlargement phenotype together with the documented functions to inhibit CM proliferation *in vitro* led us to investigate the possibility that GR and VDR signaling alters CM proliferative potential during the neonatal window *in vivo* either alone or in combination with TH signaling activation.

***i. Glucocorticoid and vitamin D receptor activation inhibit neonatal mouse cardiomyocyte proliferation in vitro.***

We first examined if GR and VDR activation regulates neonatal CM proliferation *in vitro*. Primary CMs were isolated from P1 mice and cultured with one of three GR agonists for 48 hours: hydrocortisone, corticosterone, or dexamethasone. Proliferating CMs were positive for cTnT (gray), PCM-1 rings (red), and EdU incorporation (green) (**FIG 4**). CM proliferation is inhibited by 100 nM hydrocortisone ( $0.30 \pm 0.03\%$ ), corticosterone ( $0.15 \pm 0.1\%$ ), and dexamethasone ( $0.07 \pm 0.09\%$ ) as compared to CMs cultured without any GR agonists ( $1.22 \pm 0.44\%$ ) (**FIG 4A**). We also cultured P1 CMs with two VDR agonists: calcitriol and alfacalcidol. Neonatal CM proliferation was inhibited by 1  $\mu$ M calcitriol ( $0.42 \pm 0.15\%$ ) and alfacalcidol ( $0.35 \pm 0.05\%$ ) relative to CMs cultured without any VDR agonists ( $0.87 \pm 0.10\%$ ) (**FIG 4B**). These anti-proliferative effects of GR and VDR agonists were also observed using phospho-histone H3 (pHH3) as the marker for CM proliferation (**FIG 5A**). Furthermore, in P1 CMs dexamethasone treatment upregulated GR target genes *Pam* 2.4-fold and *Cacna1c* 3.5-fold while alfacalcidol increased the expression of a VDR target gene *Vdr* 2.3-fold (**FIG 6A&B**).

Interestingly, while P1 and P7 CMs have similar levels of baseline proliferation *in vivo* (**FIG 13A**), their proliferative potential in response to VDR activation differs. We observed that unlike in P1 CMs, activation of VDR signaling did not affect proliferation in cultured P7 CMs (**FIG 14 A-C**). It is possible that the ~60% downregulation of *Vdr* in the heart between birth and P7 may explain this differential response [74] (**FIG 6D**). In contrast to our finding, calcitriol was

previously reported to induce robust proliferation of zebrafish CMs and cultured P7 mouse CMs<sup>10</sup>. The differential response of P7 CMs to VDR activation in different groups is intriguing and merits further investigation. Nonetheless, the aforementioned *in vitro* suppression of neonatal CM proliferation led us to investigate the *in vivo* contribution of GR and VDR to cardiomyocyte proliferative potential during the neonatal window.

**ii. Glucocorticoid and vitamin D receptors in cardiomyocytes are dispensable for the regulation of neonatal mouse cardiomyocyte proliferation and binucleation *in vivo*.**

To elucidate the physiological role of GR in regulating neonatal CM proliferative potential *in vivo*, we generated *Myh6-Cre;Gr<sup>ff</sup>* knockout mice in which CM-specific CRE recombinase (*Myh6-Cre*) deletes the *Gr* gene (also named as Nuclear Receptor Subfamily 3 Group C member 1, *Nr3c1*), resulting in CM-specific loss of GR signaling (**FIG 7A**). We examined heart phenotypes at P14 when most mouse CMs have completed binucleation and withdrawn from the cell cycle [26]. Interestingly, unlike our *in vitro* primary CMs, no changes of CM proliferative activity *in vivo* were observed at P14 (**FIG 7B-D**). *Myh6-Cre;Gr<sup>ff</sup>* knockout mice did not show an increase in the heart weight to body weight ratio ( $6.21 \pm 0.16$ ) compared to littermate controls ( $6.16 \pm 0.18$ ) (**FIG 7B**). Additionally, P14 *Myh6-Cre;Gr<sup>ff</sup>* hearts were comparable to littermate control hearts in terms of mononuclear CM percentage ( $13.6 \pm 1.1\%$  vs  $13.7 \pm 2.0\%$ ) ((**FIG 7C**) and (**FIG 8**)). Analysis of CM proliferation using the Ki67 marker also showed no increase in Ki67<sup>+</sup> CMs in mutant hearts ( $1.23 \pm 0.55\%$  vs  $1.09 \pm 0.23\%$ ) (**FIG 7D**). No difference was observed between control and mutant hearts when CM mitosis (positive for pHH3) and cytokinesis (Aurora B kinase at the cleavage furrow) were analyzed ((**FIG 9A&C**)). Altogether, we did not observe that CM-specific loss of GR affects CM proliferative potential during this window.

To investigate the contribution of VDR to the control of neonatal CM proliferative

potential *in vivo*, we generated mice with CM-specific loss of VDR (*Myh6-Cre;Vdr<sup>ff</sup>*) (**FIG 10A**). As with GR deletion, no changes in CM proliferative activity were observed at P14 (**FIG 10B-D**). The heart weight to body weight ratio did not significantly differ between *Myh6-Cre;Vdr<sup>ff</sup>* knockout mice compared to littermate controls (**FIG 10B**). Additionally, P14 *Myh6-Cre;Vdr<sup>ff</sup>* hearts did not significantly differ from littermate control hearts in terms of mononuclear CM percentage ( $15.8 \pm 3.2\%$  vs  $14.0 \pm 1.0\%$ ), Ki67<sup>+</sup> CM proliferation ( $0.93 \pm 0.29\%$  vs  $0.61 \pm 0.11\%$ ) ((**FIG 10C&D**) and (**FIG 8**)), CM mitosis or cytokinesis (**FIG 9A&C**). As with GR loss, VDR loss alone did not affect neonatal CM proliferative potential *in vivo*.

**iii. Loss of glucocorticoid or vitamin D receptor does not enhance cardiomyocyte proliferation potential in mice with deficiency in thyroid hormone signaling *in vivo*.**

It is plausible that the potential inhibitory effect of GR and VDR activation on CM proliferation *in vivo* is masked by other major regulators. One such candidate is TH receptor. We previously showed that TH signaling activation suppresses CM proliferative potential<sup>44</sup> (**FIG 2**), and mice with deficiency in TH receptor activation in CMs show enhanced CM proliferation and have ~30% mononuclear CMs at P14 (**FIG 3**). However, the majority of CMs in the TH receptor deficient heart still become binucleated and arrested in the cell-cycle, implicating the existence of other pathways that contribute to CM binucleation and cell-cycle withdrawal in the neonatal period. We next investigated whether loss of GR or VDR signaling affect neonatal CM proliferative potential in combination with loss of TH signaling. We bred *Myh6-Cre;Thra<sup>DN/+</sup>;Gr<sup>ff</sup>* mice that express dominant negative TH receptor alpha (THRA<sup>DN</sup>) and delete *Gr* specifically in CMs (**FIG 11A**). The heart weight to body weight ratio for *Myh6-Cre;Thra<sup>DN/+</sup>;Gr<sup>ff</sup>* ( $7.28 \pm 0.05$ ) did not significantly differ from littermate *Myh6-Cre;Thra<sup>DN/+</sup>;Gr<sup>f/+</sup>* controls ( $7.61 \pm 0.55$ ) (**FIG 11B**). Additionally, compound mutant hearts did not display significant increases in CM proliferation ( $3.5 \pm 0.7\%$  vs  $3.2 \pm 0.7\%$ ) or CM nucleation ( $32.7 \pm 8.7\%$  vs  $33.4 \pm 6.1\%$ ) compared to littermate *Myh6-Cre;Thra<sup>DN/+</sup>;Gr<sup>f/+</sup>* controls at P14 ((**FIG 11C&D**) and (**FIG 8**)). No

difference was observed between control and mutant hearts when CM mitosis and cytokinesis were examined (**FIG 9A&C**). Thus, we did not observe any significant effect of GR loss on top of TH signaling suppression on *in vivo* neonatal CM proliferative potential.

Finally, we bred *Myh6-Cre;Thra<sup>DN/+</sup>;Vdr<sup>ff</sup>* mice and observed no significant difference in the heart weight to body weight ratio ( $6.83 \pm 0.14$  vs  $7.23 \pm 0.83$ ), CM nucleation ( $24.4 \pm 2.3\%$  vs  $26.9 \pm 3.4\%$ ), or CM proliferation ( $3.0 \pm 0.3$  vs  $3.9 \pm 1.0\%$ ) compared to *Myh6-Cre;Thra<sup>DN/+</sup>;Vdr<sup>+/+</sup>* littermate controls at P14 ((**FIG 12A-D**) and (**FIG 8**)). Both mutant and control mice have similar levels of CM mitosis and cytokinesis (**FIG 9A&C**). As such, we did not observe a significant effect of VDR loss on neonatal CM proliferative potential on top of TH signaling suppression. Overall, our results show that although GR and VDR activation in cultured P1 CMs is sufficient to inhibit CM proliferation, they seem to be dispensable for CM cell-cycle exit and binucleation *in vivo* between P0 and P14.

### Chapter III – Further Exploration of Thyroid Hormone Physiology

Vertebrate thermogenic capability appears inversely correlated with cardiac regenerative potential. That is to say, tissue regeneration may generally be an ancestral vertebrate trait that was lost as adaptations like endothermy developed<sup>75</sup>. Much as neonatal mammals display increased cardiac regenerative potential compared to adults, neonates are also less able to thermoregulate than adults<sup>76</sup>. Likewise, unlike regenerative species like zebrafish and newts, non-regenerative humans and rodents can efficiently thermoregulate as adults<sup>77</sup>. While the direct effects of endothermy on cardiac regeneration remain to be explored, hypothermia has been observed to enhance brain regeneration after stroke, corroborating an inverse relationship between thermogenesis and regeneration<sup>78</sup>.

Associated with thermogenesis, metabolic CM oxidative capacity rises during early postnatal development as fetal CMs shift from glycolysis as their principal energy source to neonatal CMs which rely primarily on fatty acid  $\beta$ -oxidation, coinciding with neonatal CM terminal differentiation<sup>79</sup>. Indeed, chemically inhibiting this developmental transition to fatty acid oxidation with etomoxir delayed CM cell-cycle exit and polyploidization<sup>27</sup>. This shift from glycolysis to oxidative metabolism has also been observed in neonatal rabbit CMs<sup>80</sup>. Paralleling the closure of the neonatal mouse cardiac regenerative window, reactive oxygen species and the corresponding DNA damage increase in mouse CMs throughout the first week of life<sup>81</sup>. Scavenging reactive oxygen species from CMs delayed their postnatal cell-cycle exit and increased the percentage of mononuclear CMs, while augmenting reactive oxygen species accelerated CM cell cycle arrest<sup>81</sup>. Additionally, chronic hypoxia alleviates oxidative damage and induces CM mitosis in adult mice and improves regeneration following myocardial infarction in adult mice<sup>82</sup>. Developmental stage of CMs may play a role in their hypoxia sensitivity: while hypoxia increased primary neonatal rat CM proliferation *in vitro*, it decreased proliferation of fetal rat CMs *in vitro*<sup>83</sup>. While these evidence support the role of increasing thermogenesis and oxidative capacity in promoting CM cell-cycle withdrawal, studies in precocial mammals such as

sheep demonstrated that their CMs almost complete polyploidization and permanent cell-cycle arrest before birth, suggesting the existence of additional physiological triggers that shut down CM proliferative potential<sup>84</sup>.

Furthermore, our phylogenetic analysis of 41 vertebrate species showed that diploid CM constitution of the myocardium, a proxy of cardiac regenerative potential, correlates inversely with standard metabolic rate – the metabolic rate of any organism once the effects of organism size are factored out, as described by Kleiber’s Law<sup>44</sup>. Lower vertebrates with high cardiac regenerative potential and mostly diploid mononuclear CMs – zebrafish, newts, and reptiles – have standard metabolic rates an order of magnitude lower than those of endothermic eutherian mammals like rodents and humans<sup>85,86</sup>. Increasing CM ploidy during vertebrate evolution paralleled their transition from ectothermy to endothermy. Furthermore, mammalian body temperature – a key determinant of metabolic rate in mammals – also correlates inversely with mammalian diploid CM percentage<sup>44</sup>. Altogether, these results suggest that physiological thermogenic changes during the acquisition of endothermy in both development and evolution may induce CM polyploidization and cardiac regenerative potential loss.

***i. Thyroid hormone signaling and endothermy acquisition***

Given thyroid hormone’s role in shutting down cardiac regenerative potential<sup>44</sup> and its implication in the evolutionary and developmental acquisition of endothermy<sup>45–47</sup>, we sought to directly investigate the timecourse of vertebrate endothermy acquisition and how thyroid hormone signaling affects it. As previously discussed, the thermoregulatory capacity of neonatal mammals falls short of that of their adult counterparts; however, the exact timecourse along which thermoregulatory capacity increases is not well-described<sup>76,77</sup>.

As such, we first tracked the body temperature of wild-type mice from birth through weaning using a thermal camera (**FIG 15A**). Initially, we observed the mean temperature of the P0 pups from 3 separate litters to be approximately 23°C. Mean body temperature steadily increased through the first 2 weeks of life; by the end of the second week, pups had achieved

adult-level thermogenic capacity with body temperatures stabilizing and leveling off at approximately 37°C – comparable to adult mice (**FIG 15B**). In order to assess whether thyroid hormone signaling contributed to this endothermy acquisition, we dosed mice with PTU from either birth (P0) or before birth starting at E13.5. Intriguingly, while both PTU-dosed pup cohorts shared the same initial lack of thermoregulatory capability of wild-type newborns; neither PTU-dosed cohort achieved stable adult body temperature by the end of the second week of life. PTU-mediated inhibition of thyroid hormone signaling delayed the acquisition of adult-level body temperature by approximately a week in both cohorts (**FIG 15B**). Furthermore, this thermogenic capacity was unstable: while wild-type mice maintained body temperature above 37°C after weaning, PTU-treated mice lost body temperature every week after weaning until their low body temperature became fatal.

Our observations of endothermy acquisition suggest adult thermoregulatory capability is acquired during the first 2 weeks of life, corresponding to the same time window when cardiomyocytes permanently exit the cell cycle and cardiac regenerative capacity is lost. Furthermore, inhibition of thyroid hormone activity either at or before birth is sufficient to not only delay adult-level endothermy acquisition, but also to hobble thermogenic capacity long-term. As such, while not the only determinant of body temperature or endothermy acquisition, thyroid hormone seems to be a critical factor in both the acquisition and maintenance of endothermy. These observations posed the question of whether thyroid hormone signaling in a specific tissue type contributed substantially to thermogenic capacity, particularly considering how cardiomyocyte-specific loss of thyroid hormone signaling did not affect body temperature in our mutants from Aims I and II. As such, we used mouse mutant lines to specifically-inactivate thyroid hormone signaling via our dominant-negative transgene in either skeletal muscle (Mef2c-Cre), or the hypothalamus (Trpm2-Cre). We chose to investigate skeletal muscle given its known thermogenic capacity during exercise<sup>87</sup> and hypothalamus<sup>88</sup> given sympathetic innervation of thermogenic targets such as brown fat and skeletal muscle. However, we

observed no difference in adult body temperature between either cohort or control mice, underscoring the need for further investigation of thyroid hormone's mechanistic contribution to thermogenesis in endotherms. The apparent dispensability of thyroid hormone activity in skeletal muscle to endothermy acquisition was particularly intriguing, given our own observations of the importance of thyroid hormone in the acquisition of endothermy<sup>44</sup> (**FIG 15**) and the established importance of skeletal muscle tissue in generating body heat<sup>89</sup>; this underscores the need for more study of how different body tissues can contribute to organismal thermogenesis independently of each other.

*ii. **LRRC15: a target of thyroid hormone signaling?***

Our focus on thyroid hormone's contribution to cardiomyocyte cell-cycle exit and endothermy acquisition led us to investigate potential downstream targets of thyroid hormone signaling. LRRC15 was one such prospective target: a known tumor antigen and transmembrane protein<sup>90,91</sup> with collagen-, fibronectin-, and laminin-binding domains predicted by JAX. Also according to JAX, global LRRC15 knockout mice were healthy but exhibited improved glucose tolerance and enlarged hearts. Our RNAseq data identified LRRC15 as a potential target of thyroid hormone signaling downregulated in our dominant negative mutants (**FIG 16A**). However, cardiomyocyte nucleation or proliferative potential in these LRRC15 mutants had not been explored. Ultimately, we observed modest but statistically-significant increases in mononuclear CMs and CM proliferation (16% and 1.5%, respectively) in our LRRC15 global knockout mutants, but this modest phenotype was not physiologically significant and did not warrant further exploration as a possible effector of thyroid hormone's control over cardiac regenerative potential (**FIG 16B**).



## Conclusion, discussion, and perspectives

Although vertebrate cardiac regenerative potential varies both evolutionarily across different species and developmentally throughout the life of a given species, certain common themes still emerge. Broadly, cardiac regenerative potential has decreased throughout vertebrate evolution, with more ancestral lineages such as fish and amphibians generally displaying a greater capacity to regenerate the heart than more recent lineages like mammals. The increased metabolic demands of more efficient endothermy on mammalian adults, as well as the associated CM polyploidization and permanent cell-cycle exit, are implicated in this loss of heart regeneration in adult higher vertebrates compared to their fetal stages and to lower vertebrates. Mechanistically, these effects have been exerted in part through several nuclear hormone receptors.

Mammalian cardiomyocytes undergo postnatal cell-cycle exit and polyploidization when they lose regenerative potential<sup>7,9,39–41</sup>. The intrinsic and extrinsic molecular drivers of this process have been under intensive studies<sup>4,42–46</sup>. We identified thyroid hormone signaling as a critical regulator of this loss of vertebrate regenerative potential, not only given the inverse correlative relationship between serum thyroid hormone and regenerative potential (**FIG 1**) but also due to the effects of direct perturbation of thyroid hormone signaling on CM proliferative potential. Dosing-in 5nM triiodothyronine (T3) into the water of zebrafish recovering from heart injury effectively shut down their natural cardiac regenerative potential: post-injury CM proliferation was blunted and substantial fibrotic scars were retained at the injury site where fully-regenerated heart muscle should ordinarily be (**FIG 2**). Furthermore, blocking thyroid hormone signaling in a higher vertebrate had the converse effect: whether chemically or genetically suppressed, in the absence of thyroid hormone signaling, mouse cardiomyocytes retained a higher proliferative capacity into adulthood and cardiac regeneration was partially-enabled after heart injury (**FIG 3**).

Our observation that both GR and VDR agonists inhibit proliferation of primary neonatal

mouse CMs *in vitro* ((**FIG 4**), (**FIG 5A**)) is consistent with previous reports in rodent CM culture and rodent cardiac myocyte cell lines<sup>23,24,31,32,47</sup>. GR activation inhibits neonatal rat CM proliferation and increases CM binucleation<sup>60,61</sup>. VDR activation reduces expression of both *c-myc* and PCNA protein levels, and inhibits cell proliferation in neonatal rat CM culture<sup>69</sup>. Furthermore, our observations that P1 CMs upregulate GR- and VDR-responsive genes upon GR and VDR agonist treatment (**FIG 6A&B**) and that GR and VDR antagonists can mitigate the anti-proliferative effects of their agonists (**FIG 5B**) further support that activation of these receptors themselves inhibits neonatal CM proliferation.

Unlike our observations in cultured CMs, our *in vivo* analyses did not reveal a significant role for either receptor in regulating neonatal CM proliferative potential loss: neither CM nucleation nor CM proliferation was influenced by either GR or VDR loss in P14 mice ((**FIG 7**), (**FIG 10**)). However, injecting neonatal mice with exogenous dexamethasone and alfacalcidol from birth to P7 did reduce *in vivo* CM proliferation at P7, suggesting that GR and VDR can suppress CM proliferation *in vivo* if activated beyond physiological levels (**FIG 13B**). As such, while GR and VDR signaling are sufficient to inhibit CM proliferation in culture, we did not observe their regulatory influence on CM proliferative potential to be determinative *in vivo* at physiological levels in the neonate. Moreover, we did not observe cardiomyocyte hypertrophy of these aforementioned mutant mice at P14, suggesting that the hypertrophic phenotypes described in both mutant mice<sup>71,72</sup> may develop later in the postnatal life (**FIG 9B**). Altogether, our data indicate that while agonist treatment both *in vitro* and *in vivo* can inhibit CM proliferation, GR and VDR are not physiological regulators of CM proliferation at endogenous glucocorticoid and vitamin D levels in the neonatal time window.

To further explore the contribution of GR and VDR to *in vivo* CM proliferation in the context of cardiac injury, we induced MI with coronary artery ligation in P1 mice and injected them daily with either saline, GR-agonist dexamethasone (Dex), GR-antagonist mifepristone (Mif), VDR-agonist alfacalcidol (Alfa), or VDR-antagonist PS121912 (PS) until 7 days post-

injury, which is the global CM proliferative peak after cardiac injury<sup>100</sup>. Dex-injected mice had 80% fewer proliferating CMs than saline-injected controls (**FIG 13C**). CM proliferation in none of the other conditions differed significantly from controls. These results suggest that GR activation is sufficient but not necessary to suppress CM proliferation after injury and that VDR activation is neither sufficient nor necessary to affect CM proliferation after injury.

A possible explanation between our differential observations *in vitro* and *in vivo* may be that GR and VDR signaling are not activated during the neonatal window we examined. Previously-published mouse transcriptome data supports this: neither GR targets *Pam* and *Cacna1c* nor VDR target *Vdr* are upregulated in the mouse heart at P14<sup>101</sup> (**FIG 6E-G**). Similarly, previously-published RNAseq data shows downregulation of both *Pam* and *Vdr* in the neonatal heart<sup>74</sup> (**FIG 6C&D**). Additionally, the possibility remains that there are other *in vivo* factors not present *in vitro* whose regulatory influence over CM proliferative potential is strong enough to mask any contributions from either GR or VDR signaling. Taken together, these data suggest neither GR nor VDR are strongly activated at P14 and do not contribute substantially to the neonatal loss of CM proliferative potential. While GR and VDR signaling suppress neonatal CM proliferation *in vitro*, they do not function as major triggers of neonatal CM cell-cycle withdrawal and binucleation *in vivo*.

As previously stated, one such *in vivo* factor that exerts a stronger effect on CM proliferative potential than GR or VDR may be thyroid hormone (TH). We previously established a potent inhibitory role for TH signaling over CM proliferative potential<sup>44</sup>. Still, it remained possible that GR or VDR signaling may alter the observed effects of loss of TH signaling on CM proliferative potential. When we analyzed P14 mice both expressing *Thra*<sup>DN</sup> and lacking either GR or VDR in their CMs, no significant effects of either GR or VDR loss on CM proliferative potential were observed ((**FIG 11**), (**FIG 12**), (**FIG 9A&C**)). Thus, the regulatory influence of TH over CM proliferative potential is strong enough to overpower any contributions from either GR or VDR at physiological levels. Further investigation is needed to explore the molecular and

endocrine factors that act in parallel to and downstream of thyroid hormone to establish vertebrate cardiac regenerative potential.

As further research is conducted into the mechanisms that promote or inhibit vertebrate cardiac regenerative potential and the forces that act on these mechanisms, both our collective understanding of heart regeneration and our toolkit for promoting it therapeutically will expand. Based on the state of the field, valid directions to explore in the near future include probing into the mechanisms that shut down cardiac regeneration in certain species within otherwise regeneration-capable lineages (such as in medaka within teleost fish), as well as comprehensively assessing the cardiac regenerative potential of adult mammals that may induce CM proliferation after injury – such as bats. Additionally, identifying other physiological and molecular triggers that developmentally inhibit cardiac regenerative potential would elucidate how oxygen environment, endothermy acquisition, immune responses, and cancer risks all interplay to preclude heart regeneration – and specifically whether any factors dominate the others.

## Figures

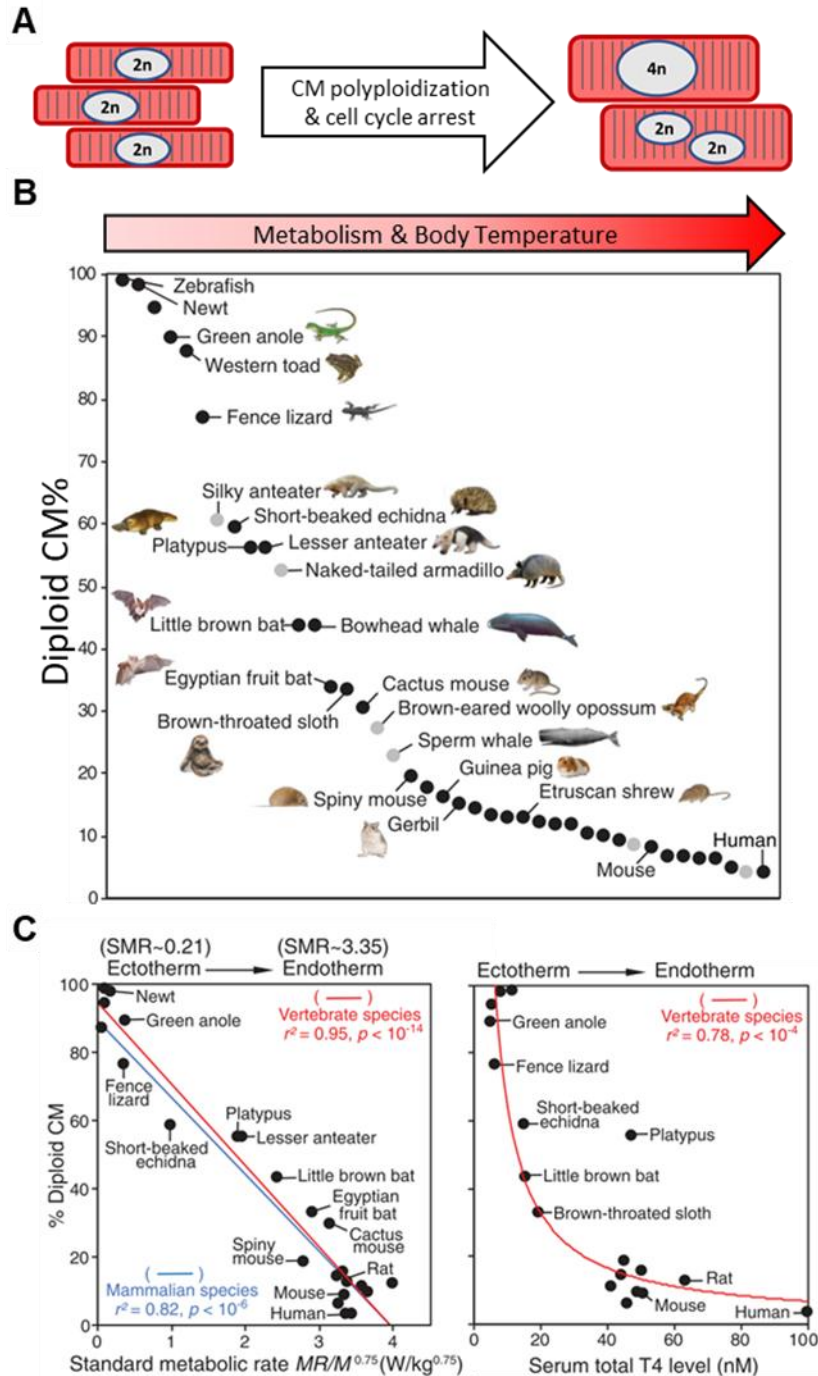


**Figure 1.1. Developmental and evolutionary cardiomyocyte transitions associated with regenerative potential loss. (A)** Diploid mononuclear (2n) proliferative CMs constitute nearly the entire regenerative myocardium while polyploid (4n+) non-proliferative CMs constitute nearly the entire non-regenerative myocardium. **(B)** Diploid CM screen of the myocardia of 41 vertebrate species. **(C)** Diploid CM percentage inversely correlates with both standard metabolic rate and serum thyroid hormone in vertebrate species.

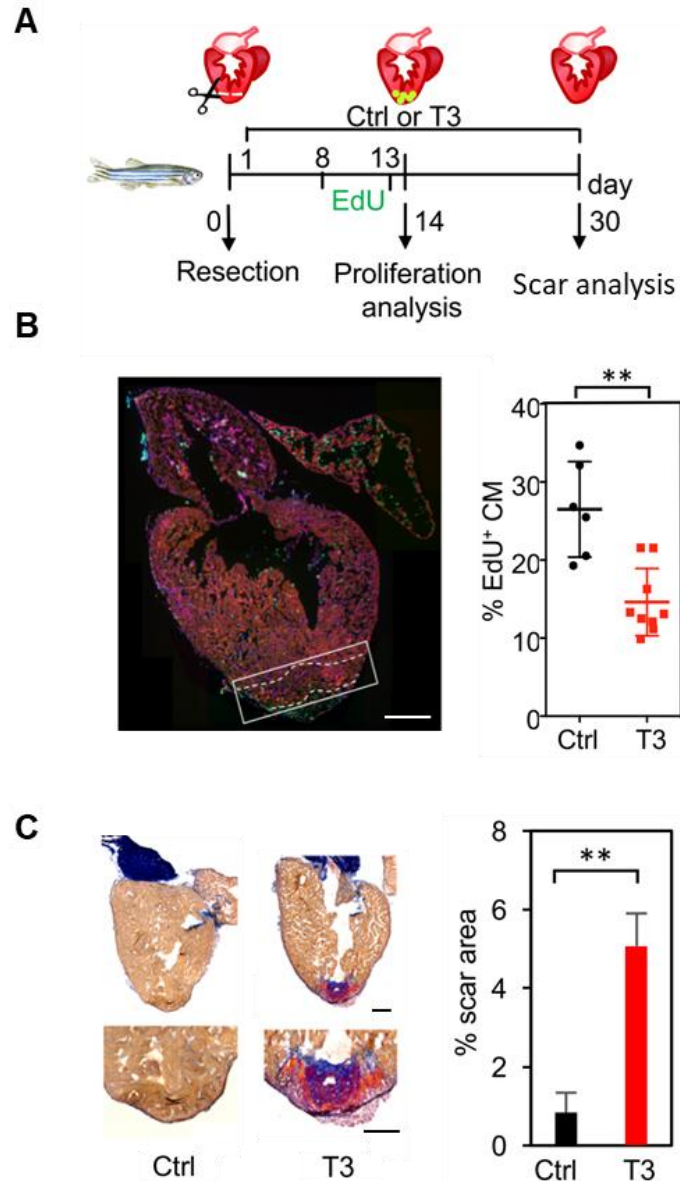


**Figure 1.2. Exogenous thyroid hormone blocks zebrafish cardiac regenerative potential *in vivo*.** (A) Schematic of zebrafish apical resection, CM proliferation analysis, and regeneration analysis timeline with or without 5nM T3. (B) Proliferation analysis 14 days after resection. CM nuclei are stained positive for MEF2. EdU- incorporated CMs are examined at the border zone within the area 100  $\mu\text{m}$  from the injury site, as marked by two dash lines in a boxed area. Magnifications of the border zone are shown in the middle with arrows pointing at EdU-positive CMs. Quantifications are presented (n=6-9 animals). (C) Heart regeneration & scar analysis 28 days after injury. Acid fuchsin orange (AFOG) stains reveal collagen in blue and fibrin in red. Presented are representative images of AFOG-stained heart sections with the fibrotic scar in blue, and quantifications of the scar area in the ventricle of control (n=17) and T3-treated (n=21) fish. Values are reported as mean  $\pm$  SEM. NS, not significant. \* $p < 0.05$ , \*\* $p < 0.01$ . Scale: 100  $\mu\text{m}$ .

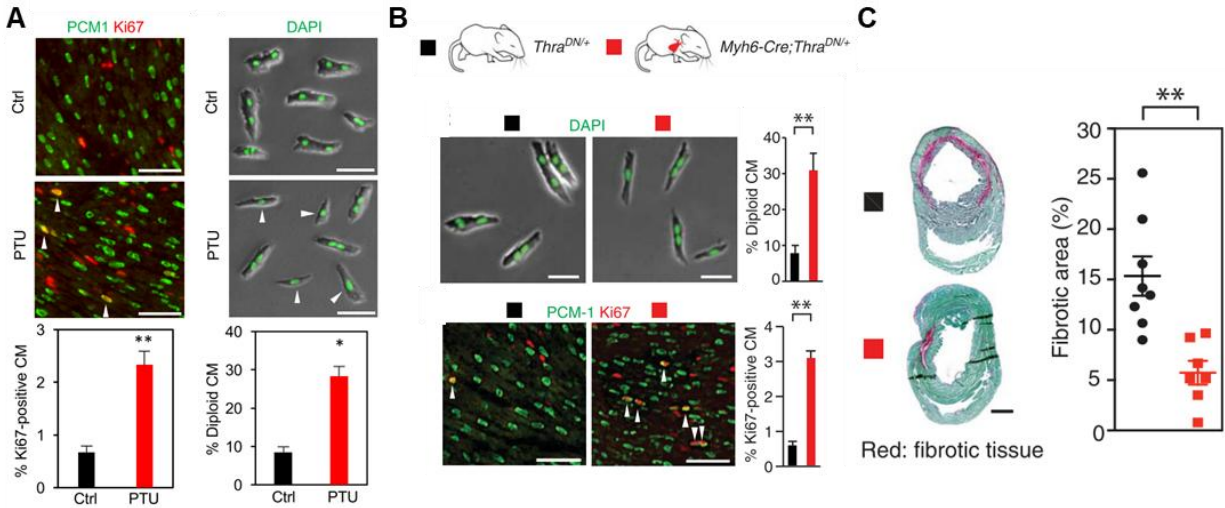


**Figure 1.3. Inactivation of CM thyroid hormone signaling enhances CM proliferation and cardiac regeneration in mice. (A)** Dietetic administration of thyroid hormone synthesis inhibitor propylthiouracil (PTU) increases CM proliferation and decreases CM ploidy in mice (n=3). **(B)** CM-specific genetic inactivation of thyroid hormone receptor via a dominant negative (DN) thyroid hormone receptor *Thra<sup>DN/+</sup>* increases CM proliferation and decreases CM ploidy in mice (n=3-7). **(C)** Fibrosis analysis 28 days after injury (n = 7 or 8 animals). Values are reported as mean  $\pm$  SEM. NS, not significant. \* $p < 0.05$ , \*\* $p < 0.01$ . Scale: 100  $\mu$ m (A & B), 1mm (C).

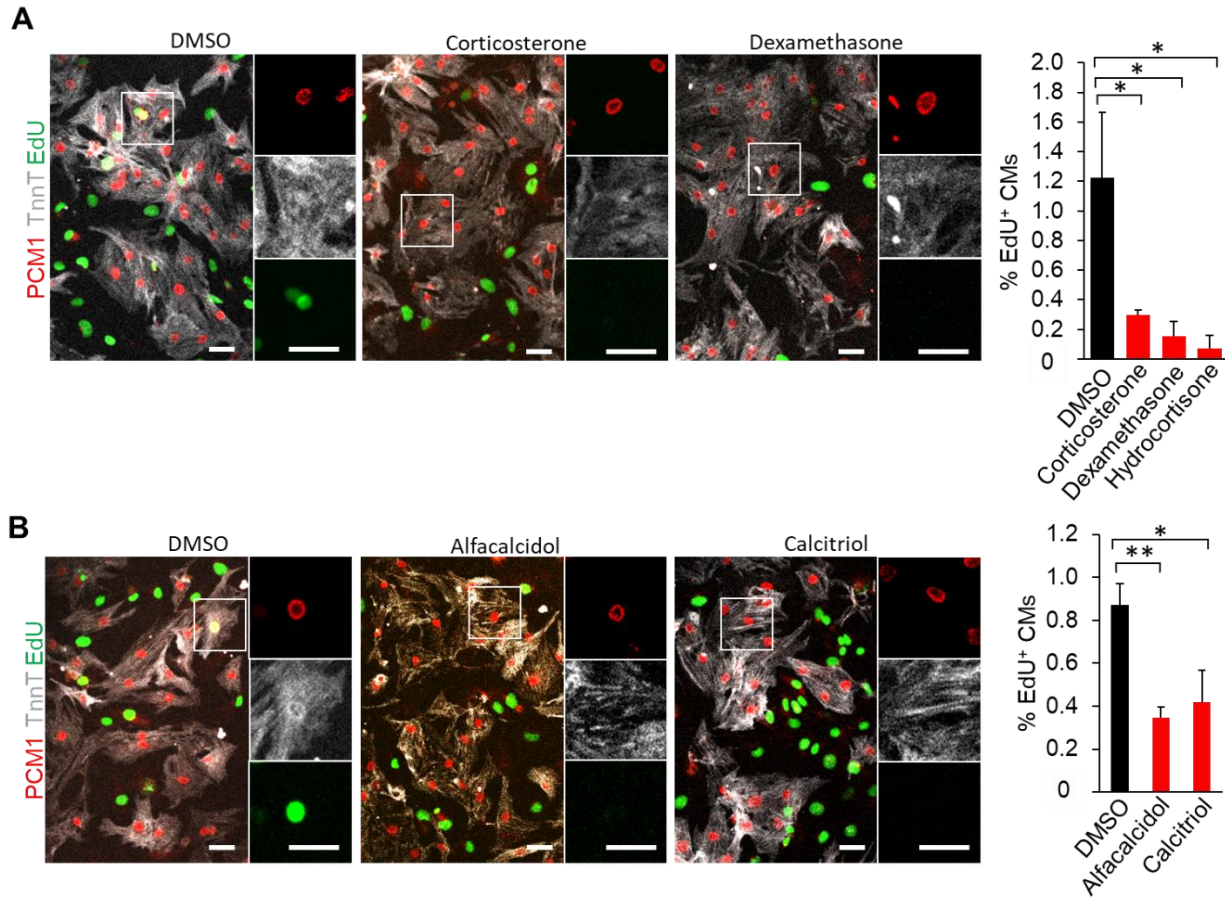


**Figure 2.1. Glucocorticoid receptor (GR) and vitamin D receptor (VDR) agonists suppress cardiomyocyte (CM) proliferative potential *in vitro*.** (A) Primary CMs (PCM1+ nuclei within TnnT+ cell bodies) cultured from P1 neonatal mice in the presence of 100 nM hydrocortisone, 100 nM corticosterone, or 100 nM dexamethasone incorporated 5-fold less EdU over 48 hr than CMs cultured without any GR agonist (DMSO). (B) Similarly, primary P1 neonatal CMs cultured with 1  $\mu$ M calcitriol and 1  $\mu$ M alfacalcidol incorporated 2-fold less EdU than those cultured with no VDR agonist (DMSO). Values are reported as mean  $\pm$  SEM (A: n=3, B: n=5). NS, not significant. \* $p < 0.05$ , \*\* $p < 0.01$ . Scale: 25  $\mu$ m.



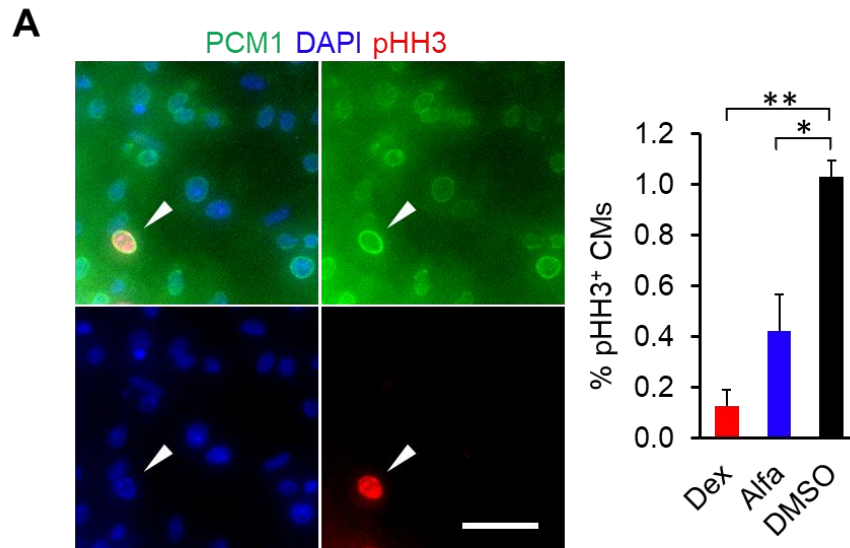


**Figure 2.2. P1 CM proliferation in various conditions. (A)** Proliferating *in vitro* P1 CMs (pHH3<sup>+</sup>) cultured with 100 nM dexamethasone (Dex), 1  $\mu$ M alfacalcidol (Alfa), and DMSO. **(B)** *In vitro* P1 CM proliferation (Ki67<sup>+</sup>) in response to 100 nM mifepristone (MIF), 100 nM mifepristone and 100 nM dexamethasone (MIF + DEX), 1  $\mu$ M PS121912 (PS), and 1  $\mu$ M PS121912 and 1  $\mu$ M alfacalcidol (PS + ALFA). Arrows indicate proliferating CM nuclei (A). Values are reported as mean  $\pm$  SEM (n=3). NS, not significant. \* $p$  < 0.05, \*\* $p$  < 0.01. Scale: 50  $\mu$ m.

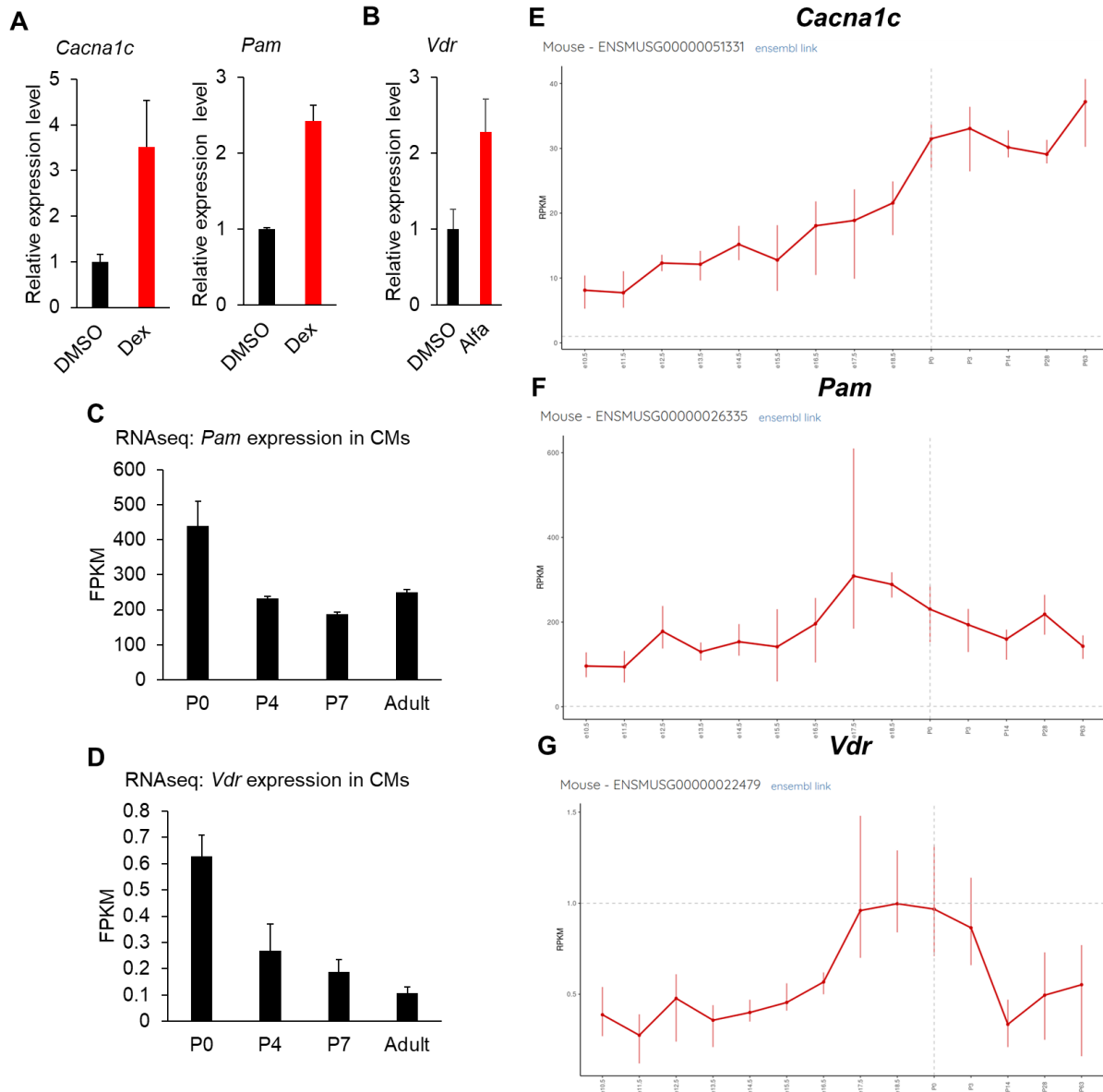


**Figure 2.3. Expression of GR and VDR downstream targets in neonatal CMs.** (A) Quantitative PCR on *in vitro* P1 CMs cultured with 100 nM dexamethasone (Dex) showed upregulation of GR targets *Pam* and *Cacna1c*. (B) Quantitative PCR on *in vitro* P1 CMs cultured with 1  $\mu$ M alfalcidol (Alfa) showed upregulation of VDR target *Vdr*. (C) RNAseq data from Online Table IA of O'Meara *et al.* 2015 (PMID: 25477501) showing developmental changes in *Pam* expression and (D) *Vdr* expression in the mouse heart. (E) Transcriptome data from the mouse heart across several developmental timepoints showing expression of *Cacna1c*, (F) *Pam*, and (G) *Vdr*. Transcriptome data were derived from the Kaessmann Lab Evo-Devo Mammalian Origins database published in Cardoso-Moreira *et al.* 2019 (PMID: 31243369). Values are reported as mean  $\pm$  SEM (n=3). (A,B)

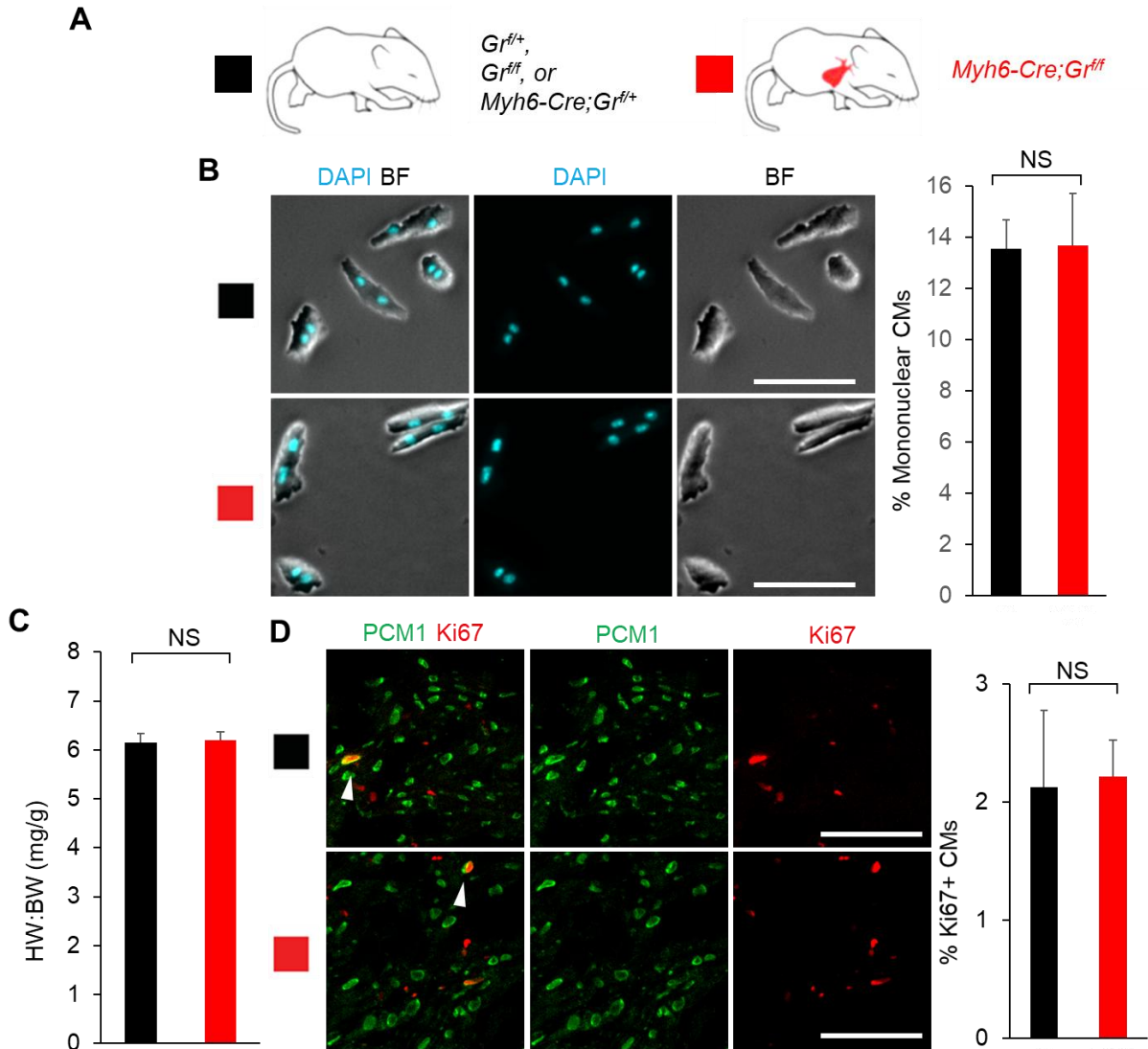


**Figure 2.4. CM-specific loss of Gr signaling does not enhance CM proliferative potential *in vivo*.** (A) Schematic for generating  $Myh6-Cre;Gr^{f/f}$  mice with CM-specific deletion of floxed endogenous GR and assessing CM proliferative potential at P14. Littermate controls included the following phenotypically-identical genotypes:  $Gr^{f/+}$ ,  $Gr^{f/f}$ , and  $Myh6-Cre;Gr^{f/+}$ . (B) Mononuclear CM percentage did not differ between  $Myh6-Cre;Gr^{f/f}$  mice and littermate controls at P14. (C) Heart weight (mg) to body weight (g) ratio (HW:BW) did not differ between  $Myh6-Cre;Gr^{f/f}$  mice and littermate controls at P14. (D) No difference in the number of  $Ki67^+$  CMs was observed between  $Myh6-Cre;Gr^{f/f}$  mice and littermate controls at P14. White arrows indicate  $Ki67^+$  CM nuclei. Values are reported as mean  $\pm$  SEM (n=3). NS, not significant. \* $p < 0.05$ . Scale: 100  $\mu$ m.

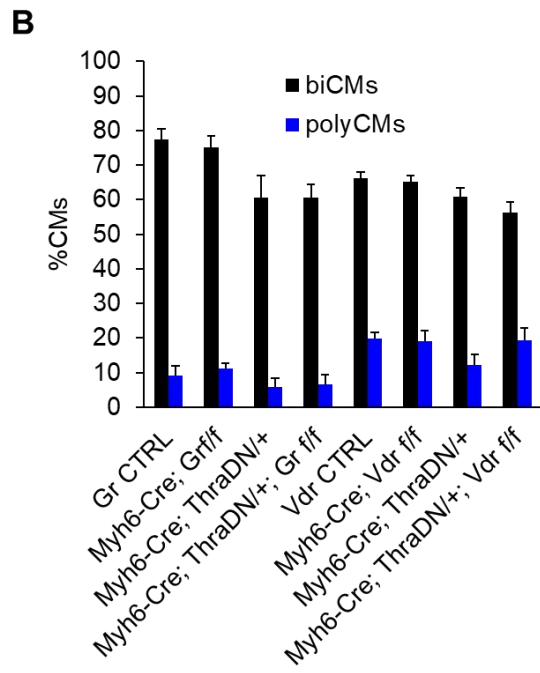
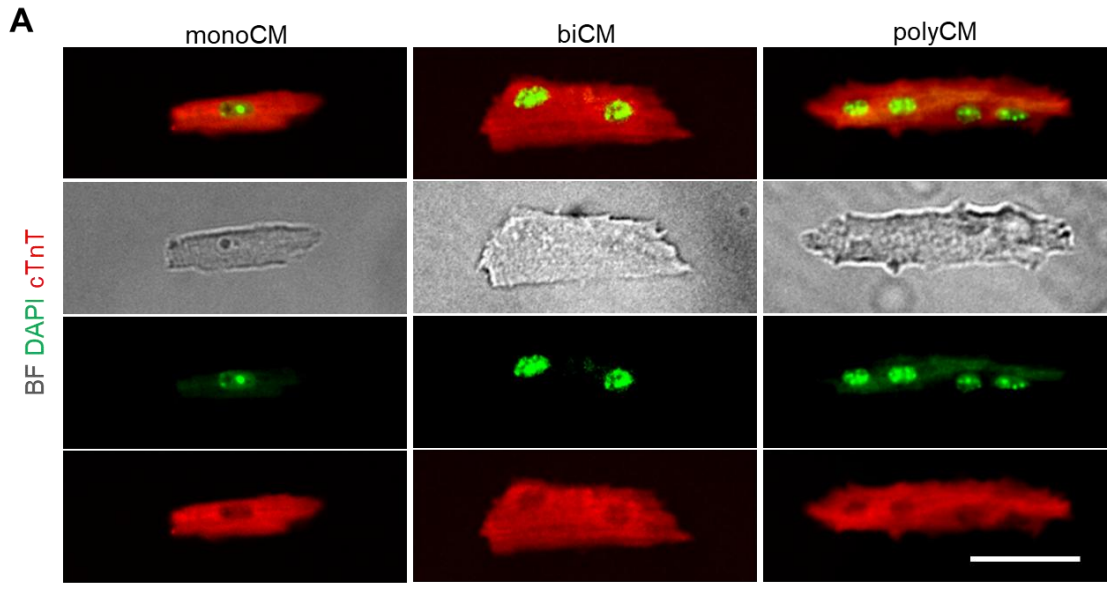


**Figure 2.5. CM nucleation at P14.** (A) Representative images of a dissociated mononuclear (monoCM), binuclear (biCM), and polynuclear (polyCM) *in vivo* CM from a wild-type P14 mouse. (B) P14 biCM% and polyCM% of the control and mutant cohorts described in Fig. 2-5. Values are reported as mean  $\pm$  SEM (n=3). Scale: 50  $\mu$ m.

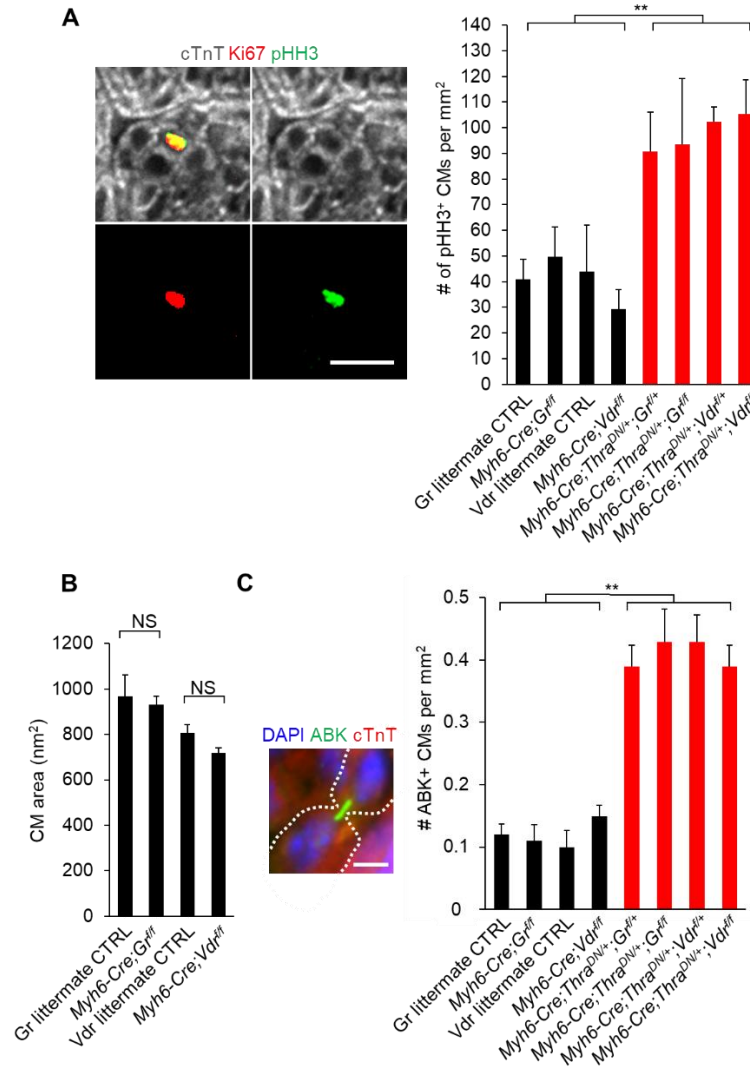


**Figure 2.6. CM-specific loss of Gr and Vdr signaling do not affect *in vivo* CM hypertrophy or CM proliferation.** (A) The average number of phosphohistone-H3<sup>+</sup> (pHH3<sup>+</sup>), Ki67<sup>+</sup> double-positive CMs per mm<sup>2</sup> area of 5  $\mu$ m heart section was not affected by Gr or Vdr loss under any conditions, but was significantly increased in all Thra<sup>DN/+</sup> cohorts. A representative pHH3<sup>+</sup>, Ki67<sup>+</sup> double-positive CM nucleus from a P14 *Myh6-Cre;Thra<sup>DN/+</sup>;Vdr<sup>ff</sup>* mouse is shown. (B) Average 2D area of dissociated CMs does not significantly differ between *Myh6-Cre;Gr<sup>ff</sup>* mice and littermate controls at P14, nor between *Myh6-Cre;Vdr<sup>ff</sup>* mice and littermate controls at P14. Littermate controls included the following phenotypically-identical genotypes: *Gr<sup>f/f</sup>*, *Gr<sup>f/+</sup>*, *Myh6-Cre;Gr<sup>f/+</sup>* for *Myh6-Cre;Gr<sup>ff</sup>* mice; and *Vdr<sup>f/f</sup>*, *Vdr<sup>f/+</sup>*, *Myh6-Cre;Vdr<sup>f/+</sup>* for *Myh6-Cre;Vdr<sup>ff</sup>* mice. (C) The average number of aurora-B kinase (ABK)<sup>+</sup> CMs per mm<sup>2</sup> area of 5  $\mu$ m heart section was not affected by Gr or Vdr loss under any conditions, but was significantly increased in all Thra<sup>DN/+</sup> cohorts. A representative ABK<sup>+</sup> CM from a P14 *Myh6-Cre;Thra<sup>DN/+</sup>;Gr<sup>ff</sup>* mouse is shown. Values are reported as mean  $\pm$  SEM (n=3). NS, not significant. \**p* < 0.05. \*\**p* < 0.01. Scale: 25  $\mu$ m (A), 5  $\mu$ m (B).

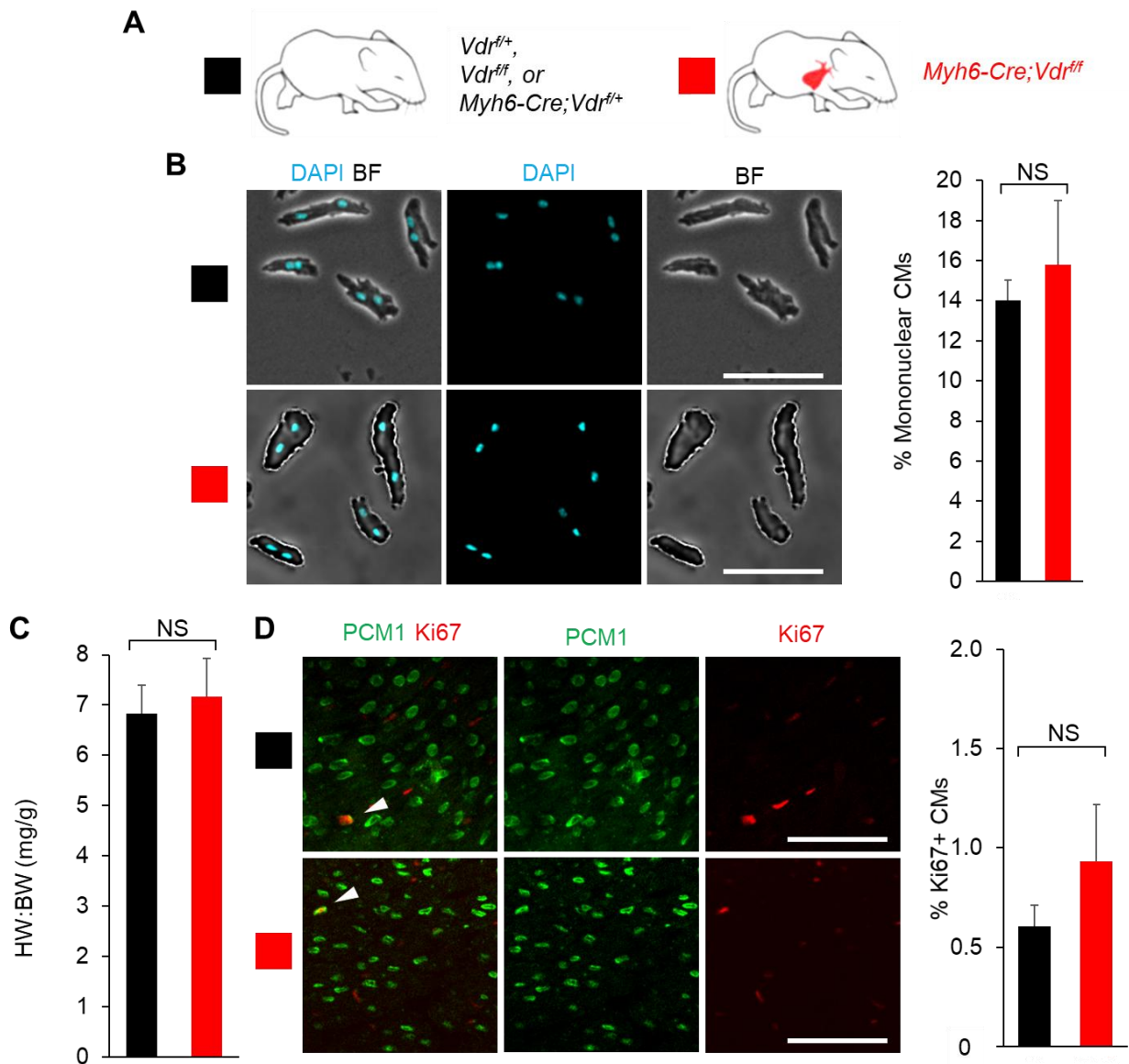


**Figure 2.7. CM-specific loss of Vdr signaling does not enhance CM proliferative potential *in vivo*.** (A) Schematic for generating  $Myh6-Cre;Vdr^{f/f}$  mice with CM-specific deletion of floxed endogenous VDR and assessing CM proliferative potential at P14. Littermate controls included three phenotypically-identical genotypes:  $Vdr^{f/f}$ ,  $Vdr^{f/+}$ , and  $Myh6-Cre;Vdr^{f/+}$ . (B) Mononuclear CM percentage did not differ between  $Myh6-Cre;Vdr^{f/f}$  mice and littermate controls at P14. (C) Heart weight (mg) to body weight (g) ratio (HW:BW) did not differ between  $Myh6-Cre;Vdr^{f/f}$  mice and littermate controls at P14. (D) No difference in the number of  $Ki67^+$  CMs was observed between  $Myh6-Cre;Vdr^{f/f}$  mice and littermate controls at P14. White arrows indicate  $Ki67^+$  CM nuclei. Values are reported as mean  $\pm$  SEM (n=3). NS, not significant. \* $P < 0.05$ . Scale: 100  $\mu$ m.



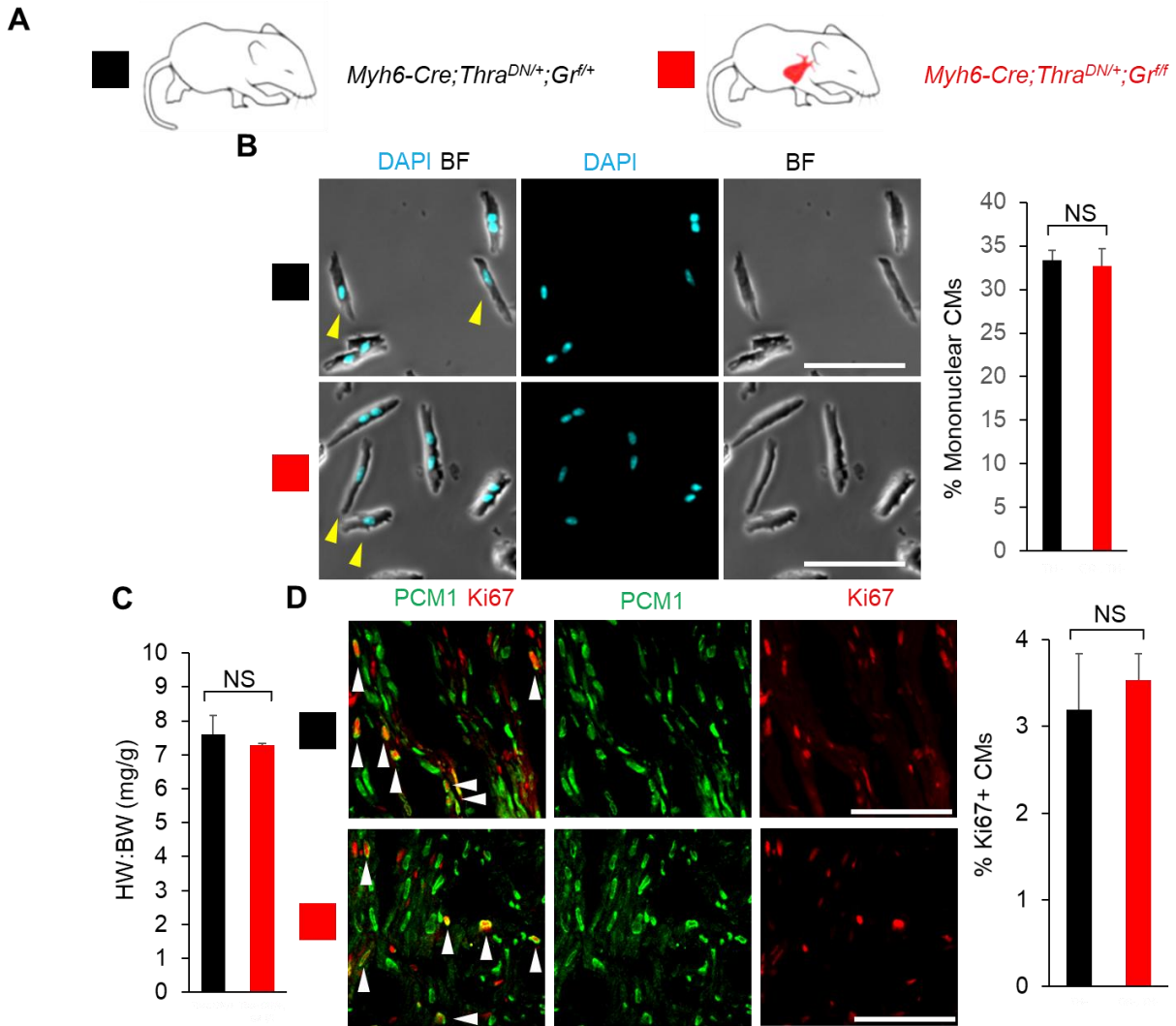


**Figure 2.8. Loss of *Gr* is insufficient to alter the *in vivo* proliferative potential retained by thyroid hormone (TH) signaling-deficient CMs.** (A) Schematic for generating *Myh6-Cre;Thra<sup>DN/+</sup>;Gr<sup>f/f</sup>* mice with CM-specific deletion of floxed endogenous GR and CM-restricted expression of a dominant negative (DN) TH receptor alpha. (B) Mononuclear CM percentage did not differ between *Myh6-Cre;Thra<sup>DN/+</sup>;Gr<sup>f/f</sup>* mice and *Myh6-Cre;Thra<sup>DN/+</sup>;Gr<sup>f/+</sup>* controls at P14. (C) Heart weight (mg) to body weight (g) ratio (HW:BW) did not differ between *Myh6-Cre;Thra<sup>DN/+</sup>;Gr<sup>f/f</sup>* mice and *Myh6-Cre;Thra<sup>DN/+</sup>;Gr<sup>f/+</sup>* controls at P14. (D) No difference in the number of Ki67<sup>+</sup> CMs was observed between *Myh6-Cre;Thra<sup>DN/+</sup>;Gr<sup>f/f</sup>* mice and *Myh6-Cre;Thra<sup>DN/+</sup>;Gr<sup>f/+</sup>* controls at P14. Yellow arrows indicate mononuclear CMs. White arrows indicate Ki67<sup>+</sup> CM nuclei. Values are reported as mean  $\pm$  SEM (n=3). NS, not significant. \* $p < 0.05$ . Scale: 100  $\mu$ m.

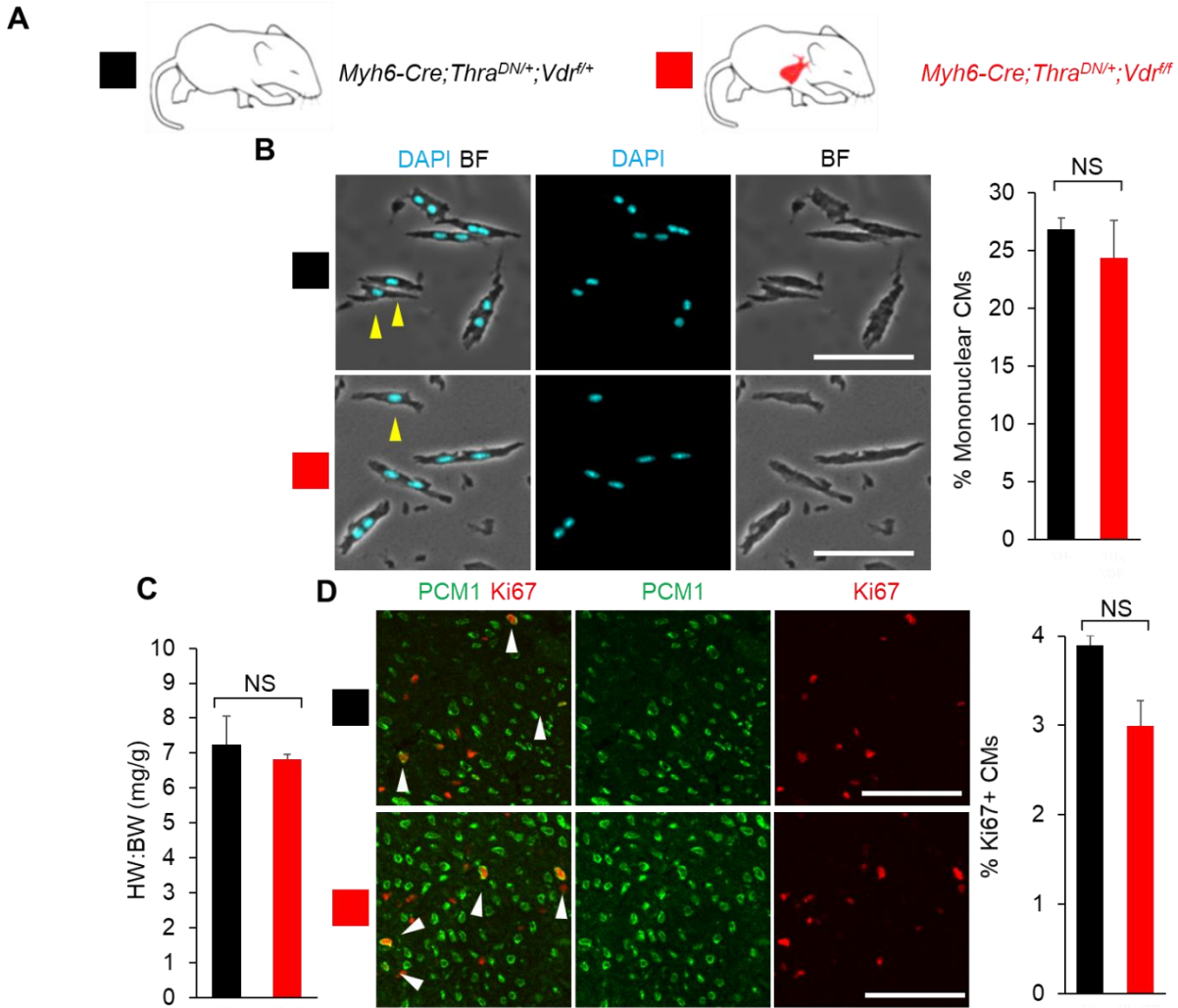


**Figure 2.9. Loss of Vdr is insufficient to alter the *in vivo* proliferative potential retained by thyroid hormone (TH) signaling-deficient CMs.** (A) Schematic for generating *Myh6-Cre;Thra<sup>DN/+</sup>;Vdr<sup>f/f</sup>* mice with CM-specific deletion of floxed endogenous VDR and CM-restricted expression of a dominant negative (DN) TH receptor alpha. (B) Mononuclear CM percentage did not differ between *Myh6-Cre;Thra<sup>DN/+</sup>;Vdr<sup>f/f</sup>* mice and *Myh6-Cre;Thra<sup>DN/+</sup>;Vdr<sup>f/+</sup>* controls at P14. (C) Heart weight (mg) to body weight (g) ratio (HW:BW) did not differ between *Myh6-Cre;Thra<sup>DN/+</sup>;Vdr<sup>f/f</sup>* mice and *Myh6-Cre;Thra<sup>DN/+</sup>;Vdr<sup>f/+</sup>* controls at P14. (D) No difference in the number of Ki67<sup>+</sup> CMs was observed between *Myh6-Cre;Thra<sup>DN/+</sup>;Vdr<sup>f/f</sup>* mice and *Myh6-Cre;Thra<sup>DN/+</sup>;Vdr<sup>f/+</sup>* controls at P14. Yellow arrows indicate mononuclear CMs. White arrows indicate Ki67<sup>+</sup> CM nuclei. Values are reported as mean  $\pm$  SEM. (n=3) NS, not significant. \**p* < 0.05. Scale: 100  $\mu$ m.



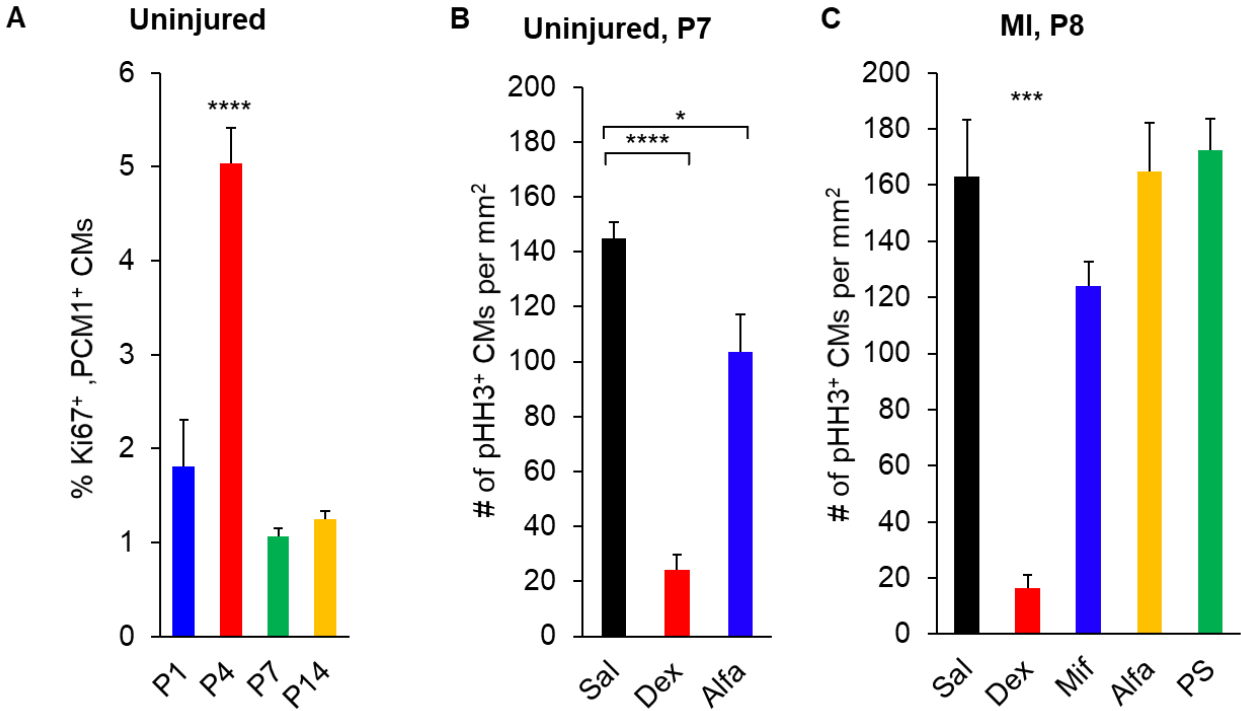


**Figure 2.10. Neonatal CM proliferation varies across developmental state and drug treatments.** (A) Developmental timecourse analysis of *in vivo* neonatal CM proliferation. The percentage of Ki67<sup>+</sup> CMs (PCM1<sup>+</sup> rings) in 5  $\mu$ m heart sections were quantified at P1, P4, P10, and P14 in wild-type mice. (B) Co-staining of pHH3 and Ki67 within cardiac troponin-t (cTnT) indicated proliferating CMs. The average number of proliferating CMs per mm<sup>2</sup> in uninjured P7 neonatal mice injected daily with either Saline (Sal), Dexamethasone (Dex), or Alfacalcidol (Alfa) from birth. (C). Co-staining of pHH3 and Ki67 within cTnT indicated proliferating CMs. The average number of proliferating CMs per mm<sup>2</sup> in P8 neonatal mice given surgically-induced myocardial infarction (MI) at P1 and subsequently injected daily with either Sal, Dex, Alfa, Mifepristone (Mif), or PS121912 (PS). Values are reported as mean  $\pm$  SEM (n = 5-7). NS, not significant. \* $p < 0.05$ , \*\* $p < 0.01$ , \*\*\*\* $p < 0.0001$ .

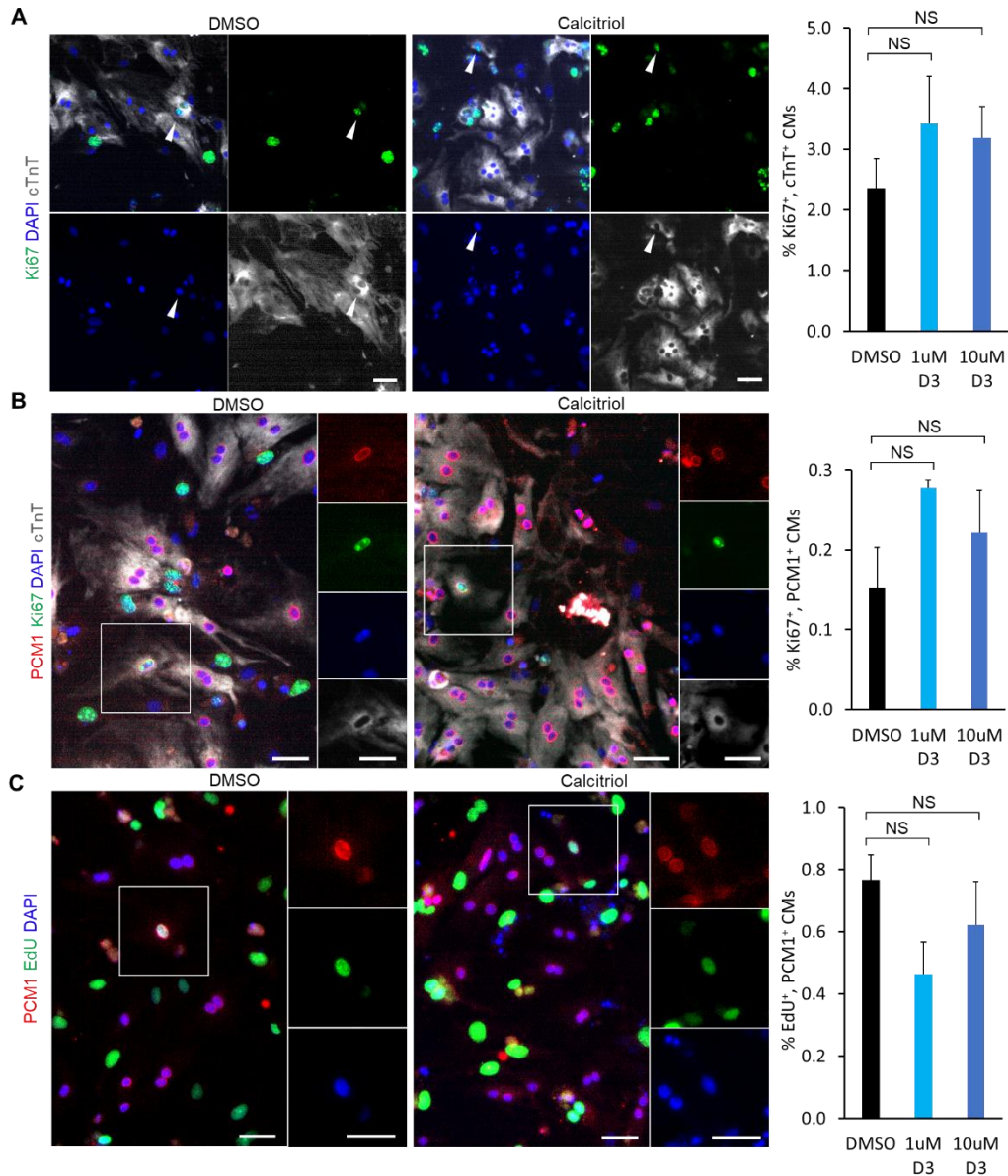


**Figure 2.11. VDR agonist does not increase proliferation in P7 CMs. CM proliferation quantifications and representative images of neonatal day 7 (P7) mouse CMs cultured with calcitriol (D3) or DMSO for 72 hr. Three different CM staining and proliferation standards were utilized. (A)** Cardiac troponin-t (cTnT) is a marker for CM cell bodies and Ki67 is a nuclear marker of cell cycle progression. Co-staining of Ki67 and DAPI inside of cTnT indicated proliferating CMs. Using this method, VDR agonist D3 did not significantly increase CM proliferation *in vitro*. **(B)** PCM1 localizes to the nuclear membrane in CMs, forming a shell around CM nuclei. Co-staining of Ki67, DAPI, and a PCM1 shell indicated proliferating CMs. D3 did not significantly increase CM proliferation *in vitro* using this quantification method. **(C)** Using EdU as a proliferation marker, D3 also did not increase PCM1<sup>+</sup> CM proliferation. Three biological replicate experiments were performed with three technical repeats for each quantification condition. Arrows indicate proliferating CM nuclei. Values are reported as mean  $\pm$  SEM (n=3). NS, not significant. Scale: 50  $\mu$ m.

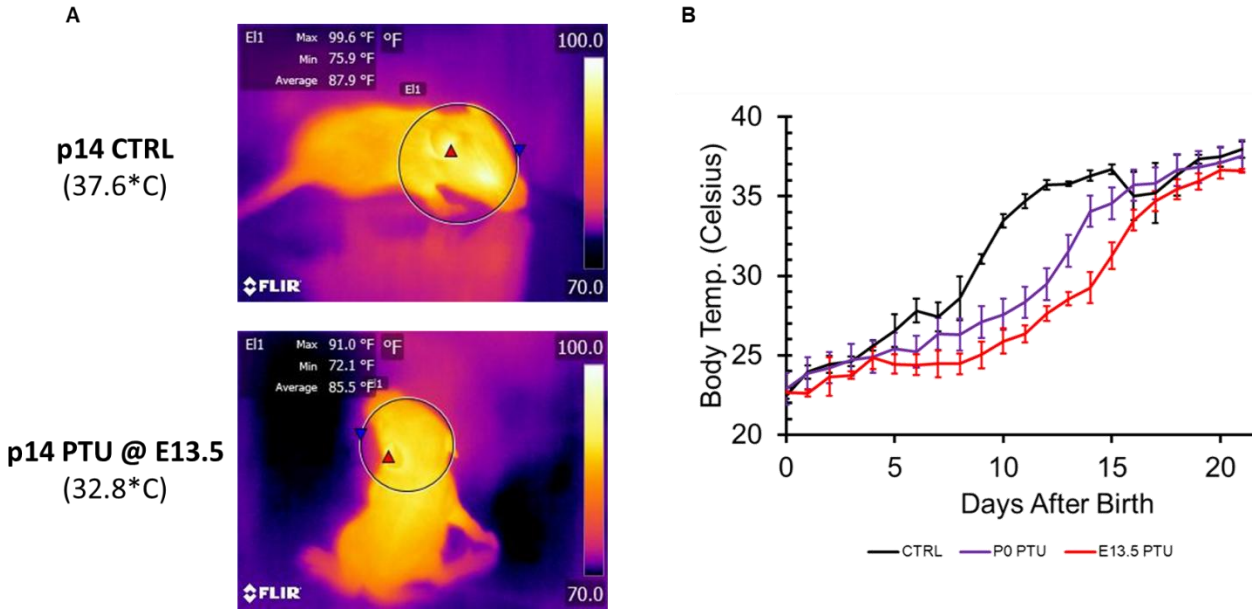


**Figure 3.1. Endothermy acquisition timecourse in neonatal mice. (A)** Representative thermal images of p14 mice taken with FLIR camera to measure body temperature after equilibration. **(B)** Body temperature curves of control and PTU-treated neonate litters. 3 litters were tracked per curve, with each daily body temperature corresponding to averaging 5 randomly-chosen pups from that litter that day. Values are reported as mean  $\pm$  SEM.

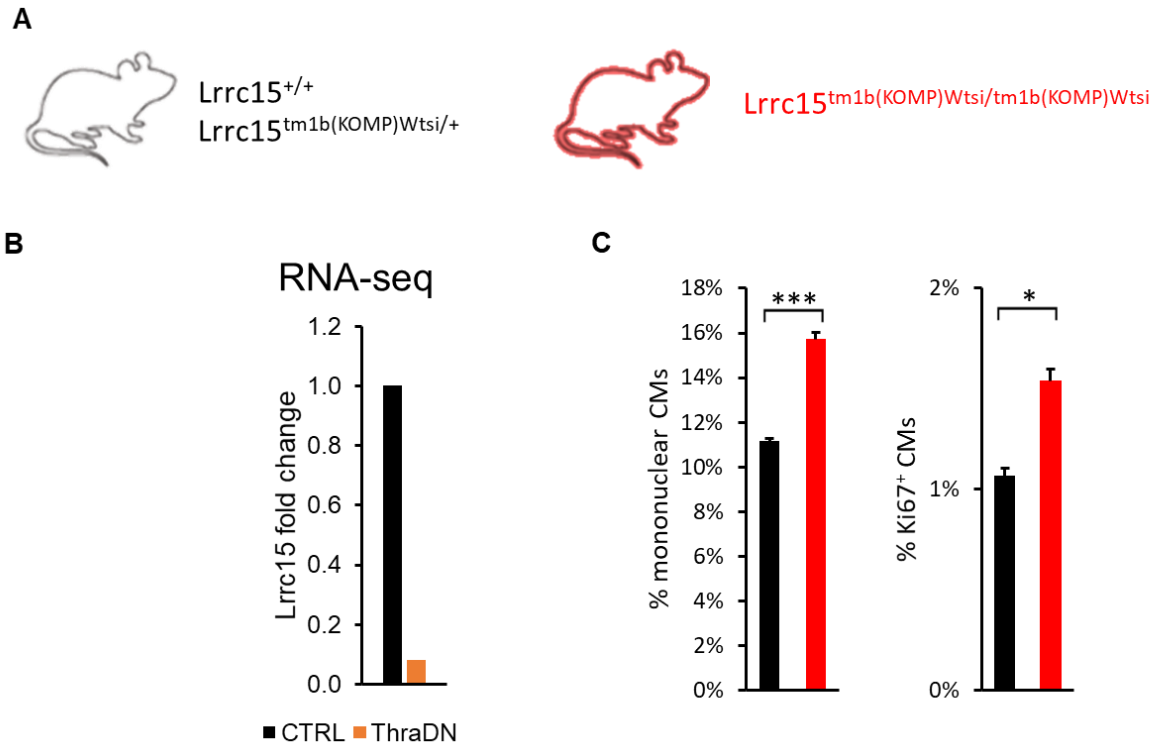


**Figure 3.2. LRRC15 exerts mild influence over cardiac regenerative potential. (A)** Schematic of global LRRC15 transgenic knockout. **(B)** CM RNA-seq data indicating reduction of LRRC15 expression in absence of thyroid hormone signaling. **(C)**. Global loss of LRRC15 has extremely modest effect on CM nucleation and proliferation. Values are reported as mean  $\pm$  SEM ( $n = 5-7$ ). NS, not significant. \* $p < 0.05$ , \*\* $p < 0.01$ , \*\*\*\* $p < 0.0001$ .

## Methods

Zebrafish surgery, treatment, and analysis: We performed 20% ventricular resections on Danio rerio (EKW background) aged 1-2 years. We then randomly assigned the fish to recover either in standard water tanks or in water tanks dosed with TH in the form of T3 in order to track post-injury CM proliferation and post-injury regeneration. For T3 treatment, fish were placed in 2L static tanks with 5 nM T3 at a density of no greater than 7 fish/2L. Water was changed daily for the first two weeks and then once in two days thereafter to minimize stress on the fish. Some fish were harvested to assess post-injury CM proliferation. In these fish, EdU injections were performed at 8 days post-injury and hearts were harvested at 14 days post-injury. We observed a 45% reduction in CM proliferation in T3-treated fish at 14 days post-injury (**FIG 2**). Furthermore, heart fibrosis was determined by acid fuchsin orange G (AFOG) staining 30 days post-apical resection in the remaining zebrafish. T3-treated zebrafish retained substantial scars rather than complete regeneration at the ventricular apex, with over 5-fold greater fibrotic area than control fish (**FIG 2**). These results demonstrate that exogenous TH inhibit zebrafish cardiomyocyte proliferation and regeneration after myocardial injury and suggest an evolutionarily-conserved function of TH in regulating cardiomyocyte proliferation.

Generating mouse lines: Mice heterozygous for the *Tg(Myh6-Cre)2182Mds* transgene (here referred to as “*Myh6-Cre*”) were bred with mice homozygous for the *Nr3c1<sup>ff</sup>* allele (here named *Gr<sup>ff</sup>*) to generate *Myh6-Cre;Gr<sup>ff/+</sup>* mice. These *Myh6-Cre;Gr<sup>ff/+</sup>* mice were then bred with *Gr<sup>ff</sup>* mice to generate mutant *Myh6-Cre;Gr<sup>ff/ff</sup>* mice and littermate controls of the following genotypes: *Gr<sup>ff/+</sup>*, *Gr<sup>ff/ff</sup>*, and *Myh6-cre;Gr<sup>ff/+</sup>*. Similarly, mice heterozygous for *Myh6-Cre* were bred with mice homozygous for the *Vdr<sup>ff</sup>* allele to generate *Myh6-Cre;Vdr<sup>ff/+</sup>* mice. These *Myh6-Cre;Vdr<sup>ff/+</sup>* mice were then bred with *Vdr<sup>ff</sup>* mice to generate mutant *Myh6-Cre;Vdr<sup>ff/ff</sup>* mice and littermate controls of the following genotypes: *Vdr<sup>ff/+</sup>*, *Vdr<sup>ff/ff</sup>*, and *Myh6-Cre;Vdr<sup>ff/+</sup>*.

In parallel, mice heterozygous for *Myh6-Cre* were bred with mice homozygous for the

*Thra*<sup>DN</sup> allele to generate *Myh6-Cre;Thra*<sup>DN/+</sup> mice that were subsequently bred with either mice homozygous for the *Gr*<sup>ff</sup> allele or mice homozygous for the *Vdr*<sup>ff</sup> allele to generate both *Myh6-Cre;Thra*<sup>DN/+;Gr</sup><sup>ff/+</sup> mice or *Myh6-Cre;Thra*<sup>DN/+;Vdr</sup><sup>ff/+</sup> mice, respectively. The *Myh6-Cre;Thra*<sup>DN/+;Gr</sup><sup>ff/+</sup> mice were bred with *Gr*<sup>ff</sup> mice to generate experimental *Myh6-Cre;Thra*<sup>DN/+;Gr</sup><sup>ff/ff</sup> mice and control *Myh6-Cre;Thra*<sup>DN/+;Gr</sup><sup>ff/+</sup> mice. The *Myh6-Cre;Thra*<sup>DN/+;Vdr</sup><sup>ff/+</sup> mice were bred with *Vdr*<sup>ff</sup> mice to generate experimental *Myh6-Cre;Thra*<sup>DN/+;Vdr</sup><sup>ff/ff</sup> mice and control *Myh6-Cre;Thra*<sup>DN/+;Vdr</sup><sup>ff/+</sup> mice.

Additionally, mice heterozygous for either *Mef2c-Cre* or *Trpm2-Cre* were bred with mice homozygous for the *Thra*<sup>DN</sup> allele to generate both *Mef2c-Cre;Thra*<sup>DN/+</sup> and *Trpm2-Cre;Thra*<sup>DN/+</sup> mice for body temperature measurements.

Analysis of cardiomyocyte nucleation: Ventricular tissues were fixed in 3.7% paraformaldehyde for 48 hours (this step was skipped for previously-fixed ventricular tissues) followed by incubation in 50% w/v potassium hydroxide solution overnight. After a brief wash with PBS, tissues were gently crushed to release dissociated cardiomyocytes. Cells were further washed with PBS three times, deposited on slides, and then allowed to dry out completely. (Note: CMs could be stained for cTnT after the last PBS wash by suspension in primary antibody solution overnight and subsequent suspension of the CMs in secondary antibody solution for 120 minutes, prior to plating on glass slides.) Nuclei were stained with 4',6-diamidino-2-phenylindole (DAPI). To determine cardiomyocyte nucleation, images of spotted cardiomyocytes were analyzed in ImageJ. The number of mononuclear, binuclear, and polynuclear cardiomyocytes was determined manually using the Count Tool. At least 130 cardiomyocytes per each sample were analyzed.

Neonatal cardiomyocyte isolation and culture: Freshly dissected ventricles from P1 or P7 CD-1 strain neonatal mice extracted and perfused with Perfusion Buffer (12 mM sodium

chloride, 1.5 mM potassium chloride, 60  $\mu$ M monopotassium phosphate, 60  $\mu$ M sodium phosphate dibasic heptahydrate, 120  $\mu$ M magnesium sulfate heptahydrate, 1mM HEPES, 4.6 mM sodium bicarbonate, 30 mM taurine, 10 mM biacetyl monoxime, 5.5 mM glucose, and 400  $\mu$ M EGTA). Cardiomyocytes were serially isolated in Digestion Buffer (2 mg/mL collagenase II and 500  $\mu$ g/mL protease XIV in perfusion buffer) for 2h at 37°C during agitation. Isolated cardiomyocytes were cultured in Plating Media (10% FBS and 100  $\mu$ g/mL primocin in DMEM) and plated on a 96-well cell culture plate at a density of ~25 thousand cells/well.

Quantitative PCR: 24 hours after plating P1 CMs, old Plating Media was changed and 5  $\mu$ M EdU Plating Media containing each drug of interest at the requisite concentration was added to each treatment well. (Control wells received Plating Media with 5  $\mu$ M EdU but no dissolved drugs.) 48 hours after drug addition, Plating Media was removed and each well was immediately washed with 100  $\mu$ L PBS before RNA was immediately isolated using TRIzol Reagent (Thermo Fisher Scientific) according to manufacturer's protocols. 100 ng RNA was used to synthesize cDNA using iScript RT Supermix (Bio-Rad 1708841) according to manufacturer's protocols. Quantitative PCR was performed using the SYBR Select Master Mix (Applied Biosystems, 4472908) and the 7900HT Fast Real-Time PCR system (Applied Biosystems). DNA content was measured via qPCR targeting GR targets *Pam* [37] and *Cacna1c* [38] and VDR target *Vdr* [68]. Relative CM DNA content was measured via normalization against CM housekeeping gene, *Actb* using the following primers: *Pam* forward = 5'- CAGAACTATCCCAGAAGAGGC-3'; *Pam* reverse = 5'- TTCTGTTTCTTTGTGATGCCCA-3'; *Cacna1c* forward = 5'- ATGAAAACACGAGGATGTACGTT-3'; *Cacna1c* reverse = 5'- ACTGACGGTAGAGATGGTTGC-3'; *Vdr* forward =5'- ACCCTGGTGACTTTGACCG-3'; *Vdr* reverse = 5'- GGCAATCTCCATTGAAGGGG-3'; *Actb* forward =5'- AGTGTGACGTTGACATCCGT-3'; *Actb* reverse = 5'- TGCTAGGAGCCAGAGCAGTA-3'.

Neonatal cardiomyocyte *in vitro* immunohistochemistry: 24 hours (48 hours for P7 CMs) after plating, old Plating Media was changed and 5  $\mu$ M EdU Plating Media containing each drug of interest at the requisite concentration was added to each treatment well. (Control wells received Plating Media with 5  $\mu$ M EdU but no dissolved drugs.) 48 hours (72 hours for P7 CMs) after drug addition, Plating Media was removed and each well was immediately washed with 100  $\mu$ L PBS, fixed with 3.7% PFA for 15 minutes at room temperature, permeabilized in 0.2% Triton X-100 in PBS (PBST), blocked in 5% normal donkey serum (NDS) in PBST for 1 hour at room temperature, and incubated with primary antibodies in PBST overnight at 4°C. After primary antibody incubation, sections were incubated in their corresponding secondary antibody for 2 hours at room temperature, and (if appropriate) the Click-it EdU imaging kit was used to visualize EdU via conjugation to sulfo-Cyanine 5-azide dye (Lumiprobe A3330). In all samples, nuclei were visualized by staining with DAPI.

Uninjured neonatal CM proliferation analysis: CD-1 littermate hearts were harvested at P1, P4, P7, and P10 for proliferation analysis.

Uninjured neonatal injections: From birth until P7, CD-1 littermates were subcutaneously injected daily with either 5  $\mu$ g dexamethasone (in 0.9% saline) per gram body weight, 1 ng alfacalcidol (in 0.9% saline) per gram body weight, or saline control. All hearts were harvested for analysis on P7.

Neonatal myocardial infarction (MI) and subsequent injections: MI injury was induced in P1 CD-1 mice via ligation of the LAD coronary artery while the animal was anesthetized on ice. After surgery, the chest wall and skin were sutured closed and animals were allowed to recover. Between P1 and P8, they were subcutaneously injected daily with either 5  $\mu$ g dexamethasone (in 0.9% saline) per gram body weight, 5  $\mu$ g mifepristone (in 0.9% saline) per gram body weight,



1 ng alfacalcidol (in 0.9% saline) per gram body weight, 1 ng PS121912 (in 0.9% saline) per gram body weight, or saline control. All hearts were harvested for analysis on P8.

*In vivo* cardiomyocyte immunohistochemistry: Experimental mice were anesthetized by injection of 20% ethyl carbamate in 1X PBS, their hearts were freshly excised, soaked briefly in 30% sucrose, and then embedded in O.C.T. Compound (Tissue Tek, cat#4583) and flash frozen on a metal block cooled by liquid nitrogen. Embedded samples were then sectioned with a Leica CM3050S to 5  $\mu$ m thickness. Tissue sections were then fixed in 3.7% paraformaldehyde for 15 min at room temperature, permeabilized in 0.2% PBST, blocked in 5% NDS in PBST for 1 hour at room temperature, and incubated with primary antibodies in PBST overnight at 4°C. After primary antibody incubation, sections were incubated in their corresponding secondary antibody for 2 hours at room temperature and mounted in DAPI to visualize nuclei.

Endothermy acquisition analysis: Propylthiouracil (PTU) was administered by feeding chow containing 0.15% PTU fed to mouse mothers either during pregnancy (E13.5) or on the day of birth (P0). For each group (untreated pups, PTU at E13.5 pups, and PTU at P0 pups), 5 pups were randomly selected from each litter each day between birth and weaning. Each pup was allowed to equilibrate its body temperature for 20 minutes in isolation in a take-out container prior to measurement of its body temperature with the FLIR thermal camera. Body temperature was recorded as peak surface temperature as indicated by the camera, always around the eyes or ears.

LRRC15 analysis: Transgenic mice ( $Lrrc15^{tm1b(KOMP)Wtsi/tm1b(KOMP)Wtsi}$  homozygotes and heterozygotes) were obtained from JAX and cardiomyocyte nucleation and proliferation analysis were performed as described above.

Statistical analysis: The number of samples per each experimental condition is listed in the description of the corresponding figure legend. Statistical significance was determined using the one-way ANOVA test (**FIG 4**), and Student's T-test for the rest of the figures.

## REFERENCES

1. Mozaffarian, D. *et al.* *Heart disease and stroke statistics-2015 update : A report from the American Heart Association. Circulation* vol. 131 (2015).
2. González-Rosa, J. M., Burns, C. E. & Burns, C. G. Zebrafish heart regeneration: 15 years of discoveries. *Regeneration* 105–123 (2017) doi:10.1002/reg2.83.
3. Witman, N., Murtuza, B., Davis, B., Arner, A. & Morrison, J. I. Recapitulation of developmental cardiogenesis governs the morphological and functional regeneration of adult newt hearts following injury. *Dev. Biol.* **354**, 67–76 (2011).
4. Vivien, C. J., Hudson, J. E. & Porrello, E. R. Evolution, comparative biology and ontogeny of vertebrate heart regeneration. *npj Regen. Med.* **1**, 16012 (2016).
5. Liao, S. *et al.* Heart regeneration in adult *Xenopus tropicalis* after apical resection. *Cell Biosci.* **7**, 1–16 (2017).
6. Poss, K. D. Heart Regeneration in Zebrafish. *Science (80- )*. **298**, 2188–2190 (2002).
7. Jopling, C. *et al.* Zebrafish heart regeneration occurs by cardiomyocyte dedifferentiation and proliferation. *Nature* **464**, 606–609 (2010).
8. Kikuchi, K. *et al.* Primary contribution to zebrafish heart regeneration by *gata4*<sup>+</sup> cardiomyocytes. *Nature* **464**, 601–605 (2010).
9. Jazwinska, A. & Sallin, P. Acute stress is detrimental to heart regeneration in zebrafish. *Open Biol.* **6**, (2016).
10. Han, Y. *et al.* Vitamin D Stimulates Cardiomyocyte Proliferation and Controls Organ Size and Regeneration in Zebrafish. *Dev. Cell* **48**, 853-863.e5 (2019).
11. González-Rosa, J. M. *et al.* Myocardial Polyploidization Creates a Barrier to Heart Regeneration in Zebrafish. *Dev. Cell* **44**, 433–446 (2018).
12. Lafontant, P. J. *et al.* The Giant Danio (*D. Aequipinnatus*) as A Model of Cardiac Remodeling and Regeneration. *Anat. Rec.* **295**, 234–248 (2012).
13. Oberpriller, J. O., Oberpriller, J. C., Arefyeva, A. M., Mitashov, V. I. & Carlson, B. M.

- Nuclear characteristics of cardiac myocytes following the proliferative response to mincing of the myocardium in the adult newt , *NotophthMmus viridescens*. *Cell Tissue Res.* **253**, 619–624 (1988).
14. Oberpriller, J. O. & Oberpriller, J. C. Response of the Adult Newt Ventricle to Injury. *J. Exp. Zool.* **187**, 249–260 (1974).
  15. Laube, F., Heister, M., Scholz, C., Borchardt, T. & Braun, T. Re-programming of newt cardiomyocytes is induced by tissue regeneration. *J. Cell Sci.* **119**, 4719–4729 (2006).
  16. Mercer, S. E. *et al.* Multi-Tissue Microarray Analysis Identifies a Molecular Signature of Regeneration. *PLoS One* **7**, (2012).
  17. Cano-Martínez, A. *et al.* Functional and structural regeneration in the axolotl heart (*Ambystoma mexicanum*) after partial ventricular amputation. *Arch. Cardiol. Mex.* **80**, 79–86 (2010).
  18. Godwin, J. W., Debuque, R., Salimova, E. & Rosenthal, N. A. Heart regeneration in the salamander relies on macrophage-mediated control of fibroblast activation and the extracellular landscape. *npj Regen. Med.* **2:22**, 1–11 (2017).
  19. Romyantsev, P. P. Post-injury DNA synthesis, mitosis and ultrastructural reorganization of adult frog cardiac myocytes - An electron microscopic-autoradiographic study. *Zeitschrift für Zellforsch. und Mikroskopische Anat.* **139**, 431–450 (1973).
  20. Romyantsev, P. P. Evidence of the regeneration of the considerable part of the frog myocardial fibers following traumatization. *Arkh. Anat. Histol. Embriol.* **40**, 65–74 (1961).
  21. Jewhurst, K. & McLaughlin, K. A. Recovery of the *Xenopus laevis* heart from ROS-induced stress utilizes conserved pathways of cardiac regeneration. *Dev. Growth Differ.* **61**, 212–227 (2019).
  22. Marshall, L. N. *et al.* Stage-dependent cardiac regeneration in *Xenopus* is regulated by thyroid hormone availability. *Proc. Natl. Acad. Sci. U. S. A.* **116**, 3614–3623 (2019).
  23. Marshall, L. *et al.* Persistent fibrosis, hypertrophy and sarcomere disorganisation after

- endoscopyguided heart resection in adult *Xenopus*. *PLoS One* **12**, 1–24 (2017).
24. Marshall, L., Girardot, F., Demeneix, B. A. & Coen, L. Is adult cardiac regeneration absent in *Xenopus laevis* yet present in *Xenopus tropicalis*? *Cell Biosci.* **8**, 1–4 (2018).
  25. Ito, K. *et al.* Differential reparative phenotypes between zebrafish and medaka after cardiac injury. *Dev. Dyn.* **243**, 1106–1115 (2014).
  26. Soonpaa, M. H., Kim, K. K., Pajak, L., Franklin, M. & Field, L. J. Cardiomyocyte DNA synthesis and binucleation during murine development. *Am. J. Physiol.* **271**, H2183–H2189 (1996).
  27. Cao, T. *et al.* Fatty acid oxidation promotes cardiomyocyte proliferation rate but does not change cardiomyocyte number in infant mice. *Front. Cell Dev. Biol.* **7**, 1–15 (2019).
  28. Porrello, E. R. *et al.* Transient Regenerative Potential of the Neonatal Mouse Heart. *Science (80-. ).* **331**, 1078–1080 (2011).
  29. Porrello, E. R. *et al.* Regulation of neonatal and adult mammalian heart regeneration by the miR-15 family. *Proc. Natl. Acad. Sci.* **110**, 187–192 (2013).
  30. Zogbi, C. *et al.* Early postnatal rat ventricle resection leads to long-term preserved cardiac function despite tissue hypoperfusion. *Physiol. Rep.* **2**, 1–11 (2014).
  31. ROBLEDO, M. Myocardial regeneration in young rats. *Am. J. Pathol.* **32**, 1215–1239 (1956).
  32. Ye, L. *et al.* Early regenerative capacity in the porcine heart. *Circulation* **138**, 2798–2808 (2018).
  33. Zhu, W. *et al.* Regenerative potential of neonatal porcine hearts. *Circulation* **138**, 2809–2816 (2018).
  34. Boulton, J. *et al.* Survival after neonatal myocardial infarction. *Pediatrics* **88**, 145 (1991).
  35. Saker, D. M., Walsh-Sukys, M., Spector, M. & Zahka, K. G. Cardiac recovery and survival after neonatal myocardial infarction. *Pediatr. Cardiol.* **18**, 139–142 (1997).
  36. Murugan, S. J., Gnanapragasam, J. & Vettukattil, J. Acute myocardial infarction in the

- neonatal period. *Cardiol. Young* **12**, 411–413 (2002).
37. Cesna, S., Eicken, A., Juenger, H. & Hess, J. Successful treatment of a newborn with acute myocardial infarction on the first day of life. *Pediatr. Cardiol.* **34**, 1868–1870 (2013).
  38. Haubner, B. J. *et al.* Functional Recovery of a Human Neonatal Heart after Severe Myocardial Infarction. *Circ. Res.* **118**, 216–221 (2016).
  39. ANTONIO P. BELTRAMI, M.D., KONRAD URBANEK, M.D., JAN KAJSTURA, PH.D., SHAO-MINYAN, M. D. & NICOLETTA FINATO, M.D., ROSSANA BUSSANI, M.D., BERNARDO NADAL-GINARD, M.D., PH.D., FURIO SILVESTRI, M.D., ANNAROSA LERI, M.D., CALBERTO BELTRAMI, M.D. PIERO ANVERSA, M. D. EVIDENCE THAT HUMAN CARDIAC MYOCYTES DIVIDE After myocardial infarction. *N. Engl. J. Med.* **344**, 1750–1757 (2001).
  40. Wang, W. E. *et al.* Dedifferentiation, Proliferation and Redifferentiation of Adult Mammalian Cardiomyocytes After Ischemic Injury. *Circulation* (2017) doi:10.1161/CIRCULATIONAHA.116.024307.
  41. Mortem, I. P., Hearts, H., Adler, C. & Costabel, U. Myocardial DNA and Cell Number Under the Influence of Cytostatics. **125**, 109–125 (1980).
  42. Brodsky, V. Y., Chernyaev, A. L. & Vasilyeva, I. A. Variability of the cardiomyocyte ploidy in normal human hearts. *Virchows Arch. B Cell Pathol. Incl. Mol. Pathol.* **61**, 289–294 (1992).
  43. Patterson, M. *et al.* Frequency of mononuclear diploid cardiomyocytes underlies natural variation in heart regeneration. *Nat. Genet.* **49**, 1346–1353 (2017).
  44. Hirose, K. *et al.* Evidence for hormonal control of heart regenerative capacity during endothermy acquisition. *Science* (80-. ). **188**, eaar2038 (2019).
  45. Hulbert, A. J. Thyroid hormones and their effects: a new perspective. *Biol. Rev. Camb. Philos. Soc.* **75**, 519–631 (2000).
  46. Little, A. G. & Seebacher, F. The evolution of endothermy is explained by thyroid

- hormone-mediated responses to cold in early vertebrates. *J. Exp. Biol.* **217**, 1642–1648 (2014).
47. Buffenstein, R., Woodley, R., Thomadakis, C., Daly, T. J. & Gray, D. A. Cold-induced changes in thyroid function in a poikilothermic mammal, the naked mole-rat. *Am. J. Physiol. Regul. Integr. Comp. Physiol.* **280**, R149-55 (2001).
  48. Li, M. *et al.* Thyroid hormone action in postnatal heart development. *Stem Cell Res.* **13**, 582–591 (2014).
  49. Maillet, M., van Berlo, J. H. & Molkentin, J. D. Molecular basis of physiological heart growth: fundamental concepts and new players. *Nat. Rev. Mol. Cell Biol.* **14**, 38–48 (2012).
  50. Liversage, R. A. & Korneluk, R. G. Serum levels of thyroid hormone during forelimb regeneration in the adult newt, *Notophthalmus viridescens*. *J. Exp. Zool.* **206**, 223–228 (1978).
  51. Chang, J. *et al.* Changes in Thyroid Hormone Levels during Zebrafish Development. *Zoolog. Sci.* **29**, 181–184 (2012).
  52. Li, M. *et al.* Core functional nodes and sex-specific pathways in human ischaemic and dilated cardiomyopathy. *Nat. Commun.* 1–12 (2020) doi:10.1038/s41467-020-16584-z.
  53. Gil-Cayuela, C. *et al.* Thyroid hormone biosynthesis machinery is altered in the ischemic myocardium: An epigenomic study. *Int. J. Cardiol.* **243**, 27–33 (2017).
  54. Gil-Cayuela, C. *et al.* Myocardium of patients with dilated cardiomyopathy presents altered expression of genes involved in thyroid hormone biosynthesis. *PLoS One* **13**, 1–12 (2018).
  55. Oakley, R. H. & Cidlowski, J. A. The biology of the glucocorticoid receptor: New signaling mechanisms in health and disease. *J. Allergy Clin. Immunol.* **132**, 1033–1044 (2013).
  56. Ronald M. Evans. The Steroid and Thyroid Hormone Receptor Superfamily on JSTOR. *Science (80- )*. **240**, 889–895 (1988).

57. Rog-Zielinska, E. A. *et al.* Glucocorticoid receptor is required for foetal heart maturation. *Hum. Mol. Genet.* **22**, 3269–3282 (2013).
58. CROCHEMORE, C., MICHAELIDIS, T. M., FISCHER, D., LOEFFLER, J.-P. & ALMEIDA, O. F. X. Enhancement of p53 activity and inhibition of neural cell proliferation by glucocorticoid receptor activation. *FASEB J.* **16**, 761–770 (2002).
59. Smith, E. *et al.* Glucocorticoids Inhibit Developmental Stage-specific Osteoblast Cell Cycle. *J. Biol. Chem.* **275**, 19992–20001 (2000).
60. Gay, M. S., Li, Y., Xiong, F., Lin, T. & Zhang, L. Dexamethasone treatment of newborn rats decreases cardiomyocyte endowment in the developing heart through epigenetic modifications. *PLoS One* **10**, 1–20 (2015).
61. Gay, M. S., Dasgupta, C., Li, Y., Kanna, A. & Zhang, L. Dexamethasone Induces Cardiomyocyte Terminal Differentiation via Epigenetic Repression of Cyclin D2 Gene. *J. Pharmacol. Exp. Ther.* **358**, 190–198 (2016).
62. Whitehurst, R. M., Zhang, M., Bhattacharjee, A. & Li, M. Dexamethasone induced hypertrophy in rat neonatal cardiac myocytes involves an elevated L-type Ca<sup>2+</sup> current. *J. Mol. Cell. Cardiol.* **31**, 1551–1558 (1999).
63. Huang, W. C. *et al.* Treatment of Glucocorticoids Inhibited Early Immune Responses and Impaired Cardiac Repair in Adult Zebrafish. *PLoS One* **8**, 1–11 (2013).
64. Bikle, D. D. Vitamin D metabolism, mechanism of action, and clinical applications. *Chem. Biol.* **21**, 319–329 (2014).
65. Ringe, J. D. & Schacht, E. Improving the outcome of established therapies for osteoporosis by adding the active D-hormone analog alfacalcidol. *Rheumatol. Int.* **28**, 103–111 (2007).
66. Samuel, S. & Sitrin, M. D. Vitamin D's role in cell proliferation and differentiation. *Nutr. Rev.* **66**, (2008).
67. Hlaing, S. M. *et al.* 1,25-Vitamin D3 promotes cardiac differentiation through modulation



- of the WNT signaling pathway. *J. Mol. Endocrinol.* **53**, 303–317 (2014).
68. Nibbelink, K. A., Tishkoff, D. X., Hershey, S. D., Rahman, A. & Simpson, R. U. 1,25(OH)<sub>2</sub>-vitamin D<sub>3</sub> actions on cell proliferation, size, gene expression, and receptor localization, in the HL-1 cardiac myocyte. *J. Steroid Biochem. Mol. Biol.* **103**, 533–537 (2007).
69. O'Connell, T. D., Berry, J. E., Jarvis, A. K., Somerman, M. J. & Simpson, R. U. 1,25-Dihydroxyvitamin D<sub>3</sub> regulation of cardiac myocyte proliferation and hypertrophy. *Am. J. Physiol. Circ. Physiol.* **272**, H1751–H1758 (1997).
70. Cutie, S., Payumo, A. Y., Lunn, D. & Huang, G. N. In vitro and in vivo roles of glucocorticoid and vitamin D receptors in the control of neonatal cardiomyocyte proliferative potential. *J. Mol. Cell. Cardiol.* (2020).
71. Chen, S. *et al.* Cardiomyocyte-specific deletion of the vitamin D receptor gene results in cardiac hypertrophy. *Circulation* **124**, 1838–1847 (2011).
72. Oakley, R. H. *et al.* Essential role of stress hormone signaling in cardiomyocytes for the prevention of heart disease. *Proc. Natl. Acad. Sci.* **110**, 17035–17040 (2013).
73. Cruz-Topete, D. *et al.* Deletion of the Cardiomyocyte Glucocorticoid Receptor Leads to Sexually Dimorphic Changes in Cardiac Gene Expression and Progression to Heart Failure. *J. Am. Heart Assoc.* **8**, 1–17 (2019).
74. O'Meara, C. C. *et al.* Transcriptional reversion of cardiac myocyte fate during mammalian cardiac regeneration. *Circ. Res.* **116**, 804–815 (2015).
75. Goss, R. J. The evolution of regeneration: Adaptive or inherent? *J. Theor. Biol.* **159**, 241–260 (1992).
76. Tourneux, P. *et al.* Échanges thermiques et thermorégulation chez le nouveau-né. *Archives de Pédiatrie* vol. 16 1057–1062 (2009).
77. Ivanov, K. P. The development of the concepts of homeothermy and thermoregulation. *Journal of Thermal Biology* vol. 31 24–29 (2006).

78. Yenari, M. A. & Han, H. S. Influence of therapeutic hypothermia on regeneration after cerebral ischemia. *Front. Neurol. Neurosci.* **32**, 122–128 (2013).
79. Lopaschuk, G. D. & Jaswal, J. S. Energy metabolic phenotype of the cardiomyocyte during development, differentiation, and postnatal maturation. *J. Cardiovasc. Pharmacol.* **56**, 130–140 (2010).
80. Lopaschuk, G. D., Spafford, M. A. & Marsh, D. R. Glycolysis is predominant source of myocardial ATP production immediately after birth. *Am. J. Physiol. - Hear. Circ. Physiol.* **261**, 1698–1705 (1991).
81. Puente, B. N. *et al.* The Oxygen Rich Postnatal Environment Induces Cardiomyocyte Cell Cycle Arrest Through DNA Damage Response. *Cell* **157**, 565–579 (2014).
82. Nakada, Y. *et al.* Hypoxia induces heart regeneration in adult mice. *Nature* **541**, 222–227 (2017).
83. Sun, Y. *et al.* Effects of hypoxia on cardiomyocyte proliferation and association with stage of development. *Biomed. Pharmacother.* **118**, 109391 (2019).
84. Jonker, S. S., Louey, S., Giraud, G. D., Thornburg, K. L. & Faber, J. J. Timing of cardiomyocyte growth, maturation, and attrition in perinatal sheep. *FASEB J.* **29**, 4346–4357 (2015).
85. Makarieva, A. M. *et al.* Mean mass-specific metabolic rates are strikingly similar across life's major domains: Evidence for life's metabolic optimum. *Proc. Natl. Acad. Sci. U. S. A.* **105**, 16994–16999 (2008).
86. Schmidt-Nielsen, K., Bolis, L., Taylor, C. R., Stevens, C. E. & Bentley, P. J. *Comparative physiology: primitive mammals.* (Cambridge University Press., 1980).
87. González-Alonso, J. Human thermoregulation and the cardiovascular system. in *Experimental Physiology* vol. 97 340–346 (Blackwell Publishing Ltd, 2012).
88. Lowell, B. B. & Spiegelman, B. M. Towards a molecular understanding of adaptive thermogenesis. *Nature* vol. 404 652–660 (2000).

89. Wright, T., Davis, R. W., Pearson, H. C., Murray, M. & Sheffield-moore, M. Skeletal muscle thermogenesis enables aquatic life in the the smallest marine mammal. **225**, 223–225 (2021).
90. Wang, Y. *et al.* LRRC15 promotes osteogenic differentiation of mesenchymal stem cells by modulating p65 cytoplasmic/nuclear translocation. *Stem Cell Res. Ther.* **9**, 1–13 (2018).
91. O'Prey, J., Wilkinson, S. & Ryan, K. M. Tumor Antigen LRRC15 Impedes Adenoviral Infection: Implications for Virus-Based Cancer Therapy. *J. Virol.* **82**, 5933–5939 (2008).
92. Bergmann, O. *et al.* Dynamics of Cell Generation and Turnover in the Human Heart. *Cell* **161**, 1566–1575 (2015).
93. Soonpaa, M. H. & Field, L. J. Assessment of cardiomyocyte DNA synthesis in normal and injured adult mouse hearts. *Am. J. Physiol.* (1997).
94. Alkass, K. *et al.* No Evidence for Cardiomyocyte Number Expansion in Preadolescent Mice. *Cell* **163**, 1026–1036 (2015).
95. Senyo, S. E., Lee, R. T. & Kühn, B. Cardiac regeneration based on mechanisms of cardiomyocyte proliferation and differentiation. *Stem Cell Res.* **13**, 532–541 (2014).
96. Xin, M., Olson, E. N. & Bassel-Duby, R. Mending broken hearts: Cardiac development as a basis for adult heart regeneration and repair. *Nature Reviews Molecular Cell Biology* vol. 14 529–541 (2013).
97. Xiang, M. S. W. & Kikuchi, K. Endogenous Mechanisms of Cardiac Regeneration. in *International Review of Cell and Molecular Biology* vol. 326 (2016).
98. Foglia, M. J. & Poss, K. D. Building and re-building the heart by cardiomyocyte proliferation. *Development* **143**, 729–740 (2016).
99. Øvrebø, J. I. & Edgar, B. A. Polyploidy in tissue homeostasis and regeneration. *Development* **145**, dev156034 (2018).
100. Porrello, E. R. *et al.* Transient Regenerative Potential of the Neonatal Mouse Heart.

*Science* (80-. ). **331**, 1078–1080 (2011).

101. Cardoso-Moreira, M. *et al.* Gene expression across mammalian organ development.

*Nature* **571**, 505–509 (2019).

## Publishing Agreement

It is the policy of the University to encourage open access and broad distribution of all theses, dissertations, and manuscripts. The Graduate Division will facilitate the distribution of UCSF theses, dissertations, and manuscripts to the UCSF Library for open access and distribution. UCSF will make such theses, dissertations, and manuscripts accessible to the public and will take reasonable steps to preserve these works in perpetuity.

I hereby grant the non-exclusive, perpetual right to The Regents of the University of California to reproduce, publicly display, distribute, preserve, and publish copies of my thesis, dissertation, or manuscript in any form or media, now existing or later derived, including access online for teaching, research, and public service purposes.

DocuSigned by:

*Stephen Cutie*

A20BB944206A4AB...

Author Signature

8/27/2021

Date